VOL. 257 NOVEMBER 1959 No. 9

American Journal of Science

Established in 1818 by Benjamin Silliman

EDITORS
JOHN RODGERS—JOSEPH T. GREGORY

ASSOCIATE EDITORS

GEORGE GAYLORD SIMPSON, CAMBRIDGE, MASS.
A. F. BUDDINGTON, PRINCETON, N. J.
CARL O. DUNBAR
MATT WALTON
HENRY MARGENAU
RICHARD F. FLINT
HORACE WINCHELL
HAROLD G. CASSIDY
EDWARD S. DEEVEY, JR.
G. EVELYN HUTCHINSON
NEW HAVEN, CONN.
WILMOT H. BRADLEY
PHILIP H. ABELSON
WASHINGTON, D. C.
LEASON H. ADAMS, LOS ANGELES, CALIF.
HOWEL WILLIAMS, BERKELEY, CALIF.
C. R. LONGWELL, PALO ALTO, CALIF.
ADOLPH KNOPF, STANFORD, CALIF.
FREDERICK J. ALCOCK, OTTAWA, CANADA
CECIL E. TILLEY, CAMBRIDGE, ENGLAND

STERLING TOWER
YALE UNIVERSITY
NEW HAVEN, CONNECTICUT

Published 10 times a year. Ten dollars a year. One dollar twenty-five cents a copy.
Foreign, ten dollars sixty cents. Canada, ten dollars thirty-five cents.

AMERICAN JOURNAL OF SCIENCE

Established in 1818 by Benjamin Silliman

THE FIRST SCIENTIFIC JOURNAL IN THE UNITED STATES

DEVOTED TO THE GEOLOGICAL SCIENCES AND TO RELATED FIELDS

Editors: JOHN ROGERS—JOSEPH T. GREGORY
Managing Editor: BETH A. BROMBERT

Entered as second-class matter at the Post Office at New Haven, Conn., under the Act of March 3, 1879. Published monthly, except July and September, at Sterling Tower, Yale University, New Haven, Conn.

Subscription rate $10 per year ($1.25 a number). Student rate $5 per year (application blanks available on request). Postage prepaid to the United States; 35 cents per year to Canada; 60 cents per year elsewhere.

The JOURNAL completed its *first* series of 50 volumes in 1845, its *second* series of 50 volumes in 1870, its *third* series of 50 volumes in 1895, its *fourth* series of 50 volumes in 1920, its *fifth* series of 36 volumes in 1938. Since 1938 the numbering by series has been discontinued, and volumes are annual and bear the whole numbers as of 1818, that for 1939 being volume 237.

Back numbers and volumes, also cumulative indices of all series, may with few exceptions be obtained from the office of the AMERICAN JOURNAL OF SCIENCE, Sterling Tower, New Haven, Conn. Positive microfilm copies of each complete volume may be purchased by subscribers to the paper edition from *University Microfilms*, 313 N. First St., Ann Arbor, Michigan. Regular subscribers may purchase each past year in microcard form, from *The Microcard Foundation*, Wesleyan University, Middletown, Connecticut.

INSTRUCTIONS TO CONTRIBUTORS

Typescripts of articles submitted should be double-spaced, should follow the recommendations in the pamphlet *Suggestions to Authors*, 5th ed. (see below), and should be preceded by brief abstracts. They should be checked with special care before being submitted, to avoid changes in proof other than printer's errors.

References to literature should be listed alphabetically by authors at the end of the article; all references should be complete. For articles in journals or other serial publications, the reference should give in order: Author's name, year of publication, full title: name of periodical or series, volume number, inclusive pages. For books or other unnumbered publications, it should give: Author's name, years of publication, full title: place of publication, publisher. This form follows the recommendations in the pamphlet "Abbreviations used in publications of the U. S. Geological Survey", which is also the standard used for abbreviating names of periodicals, etc. Citations within an article should be to author and year, with specific pages wherever appropriate.

Plates (photographs), *figures* (line drawings), and *footnotes* should each be numbered consecutively through each article, using arabic numerals. If two photographs form one plate, they are figures 1 and 2 of that plate.

Illustrations should be neat and legible and should include explanations of symbols used. Copy that cannot be reproduced cannot be accepted. Plates and figures should be capable of reduction to not more than 4 by 7 inches, all lettering being at least 1/16th inch high after reduction. When necessary, one large map or table can be accepted, if it will not exceed 7 inches in width after reduction. Line drawings should be in black India ink on white drawing board, tracing cloth, or coordinate paper printed in blue. Photographs should be positive glossy prints. Photostatic and typewritten material cannot be accepted as copy for illustrations.

Reprints. Thirty separate copies of each article will be furnished to the author free of cost and without previous notice from him; these will be without a cover. Additional copies will be furnished at cost, which will of course be greater if the article is accompanied by plates involving unusual expense. Copies will be furnished with a printed cover giving the title, author, volume, page, and year, when specially ordered.

Suggestions to Authors of the Reports of the United States Geological Survey, 5th ed. Washington, D. C., 1958 (Government Printing Office, $1.75).

[American Journal of Science, Vol. 257, November 1959, P. 609-647]

American Journal of Science

NOVEMBER 1959

ROLE OF OXYGEN PRESSURE IN THE CRYSTALLIZATION AND DIFFERENTIATION OF BASALTIC MAGMA*

E. F. OSBORN

College of Mineral Industries, Pennsylvania State University, University Park, Pa.

ABSTRACT. Two types of crystallization paths in iron oxide systems are illustrated by describing equilibrium crystallization in the fayalite field of the system FeO–Fe_2O_3–SiO_2. In one type where total composition of the mixture remains constant, composition of the liquid changes along a path leading to a boundary curve and thence to an invariant point. In the other type oxygen partial pressure remains constant causing the liquid of the crystallizing mixture to follow an oxygen isobaric line on the liquidus surface. In this second type of crystallization the oxygen content of the mixture changes.

These principles are extended into an examination of crystallization phenomena in the quaternary system MgO–FeO–Fe_2O_3–SiO_2. In this system occurrence of extensive solid solution in olivine, pyroxene and magnetite structures along with incongruent melting of pyroxene necessitates consideration of fractional as well as equilibrium crystallization. It is shown that with fractional crystallization at *constant total composition* (Type I) the liquid moves to the magnetite (magnesioferrite) surface and thence down this surface continuously decreasing in amount and increasing in iron oxide content. With magnetite as one of the crystallizing phases, oxygen pressure decreases. Liquids take the same general direction of composition change as they do during fractional crystallization in the simpler system, MgO–FeO–SiO_2. Initial FeO/Fe_2O_3 ratio does not affect direction of movement of liquid after the magnetite surface is reached. With fractional crystallization at *constant oxygen partial pressure*, (Type II), the direction of movement of liquid is very different. Because the liquid must remain on an isobaric surface, change in composition of the liquid is in the direction of increasing silica and decreasing iron oxide content as soon as magnetite begins to crystallize. The liquid moves along the magnetite boundary terminating at the pyroxene-magnetite-silica univariant line, where the liquid completes its crystallization without further change of composition just as if it had reached a eutectic point. For mixtures analogous to basalt compositions, a small net increase in oxygen content is realized during the crystallization. If oxygen pressure increases during fractional crystallization, the liquid moves to even higher silica and lower iron oxide end points than under conditions of constant oxygen pressure. Thus the trend of change of liquid composition toward higher iron oxide contents during fractional crystallization of Type I shifts progressively to one of decreasing iron oxide content and increasing silica as the rate of decrease in oxygen pressure required in Type I crystallization becomes less and approaches the condition of constant or increasing oxygen pressure. The ratio of iron oxide to iron oxide plus magnesia in the fractionating liquid rises steeply with increasing silica content in Type I crystallization, and rises gently in Type II, for mixtures simulating basalt compositions.

Analyses applicable to igneous rocks are plotted for comparison with curves for fractionating liquids in the system MgO–FeO–Fe_2O_3–SiO_2. The iron oxide-magnesia trends for average tholeiitic basalts and Skaergaard liquids are of the same nature as those for liquids of Type I crystallization, whereas the basalt-andesite-dacite-rhyolite series exhibits trends of the nature of Type II crystallization. An example of the latter is the Cascade lava series. Basaltic magmas of the non-orogenic regions typically crystallize with total composition remaining essentially constant. Basaltic magmas entering the orogenic belts

* Contribution No. 58-78 from College of Mineral Industries, The Pennsylvania State University, University Park, Pennsylvania.

evidently crystallize with oxygen pressure remaining approximately constant. That this is true is further borne out by plotting subtraction diagrams. Where crystallization is of Type I, the FeO and Fe_2O_3 curves have a continuous slope, whereas with crystallization of Type II the curves for the two iron oxides have a discontinuity in slope because of addition of oxygen to the mixture during crystallization. The subtraction diagrams further suggest that high alumina basalts develop from tholeiitic olivine basalt by fractional crystallization under conditions such that plagioclase is delayed in separating from the liquid.

The tendency for oxygen pressure to decrease at a slower rate, or remain about constant or actually to increase during crystallization of basaltic magma entering orogenic belts instead of decreasing as in Type I crystallization may be the result of higher water contents of orogenic magmas coupled with their habit of accumulating in reservoirs where with slow cooling and fractional crystallization water pressure increases during crystallization. Liquids escaping from the reservoirs extrude as calc-alkali series of lavas and ash while those remaining below the surface cool as granodiorite and related plutonic rocks. The complementary crystal fraction is represented by periodotites and serpentinites.

INTRODUCTION

The manner of evolution of the igneous rocks continues to be one of the great problems of natural science. Physicochemical and geological research are being intensively applied to the problem, guaranteeing continual progress toward a solution, but one might easily conclude that we have reached only a healthy and encouraging state of confusion. Answers to many questions must be obtained before we can dispense with the "granite problem", the question of the development of tholeiite versus alkali basalt, the puzzle of the relative importance of fractional crystallization and assimilation to give the calc-alkali trend, and other mysteries of the igneous rocks where the clues have been all too few. Basic to igneous rock problems is an understanding of the precise manner in which basaltic magma crystallizes and differentiates under various conditions. I wish to direct attention to an aspect which may be very significant, namely the way in which the course of crystallization is affected by the manner of change of oxygen partial pressure.

Much continues to be written on the manner of derivation of the calc-alkali series of andesites-dacites-rhyolites and their plutonic equivalents. By the fractional crystallization of basalt at least a small amount of an end product of rhyolitic or granitic composition can be produced, but recent writers on the subject except for Bowen have in the main argued that this process is not sufficient to produce the rocks which we see. Fenner (1929, 1948) has insisted that fractional crystallization is an inadequate explanation and has advocated, among other processes, liquid immiscibility in silicate melts as possibly an important factor in the derivation of the calc-alkali series. Wager and Deer (1939) argue that fractional crystallization of basaltic magma can only take the trend established for the Skaergaard intrusion, and hence that the calc-alkali series must be "the result of the mixing of basic and acid material". Waters (1955) considers basalt ("tholeiitic magma") as the parent of the Cascades andesites, suggesting that "water, silica, alkalis, calcium and magnesium ions, and other easily removable constituents were stewed from the downbuckling sediments", and entered and mixed with the tholeiite magma to produce andesite. In Tilley's (1950) discussion of some aspects of magmatic evolution he seems driven to accept sialic contamination of basaltic magma as being necessary to provide the compositions which by fractional crystallization may continue to evolve into the andesite-rhyolite series; but he states: "In the

field of volcanic petrogenesis no more pressing problem awaits intimate investigation than this—the study of the geochemistry and the chemical variation within the basalt-andesite suites of the orogens."

The laboratory investigations especially applicable to the basalt-andesite problem have been done in the main under conditions such that the effect of the partial pressure of oxygen on crystallization could not be seen. Still Bowen (1947) recognized that atmosphere must have an important effect and for example considered that the Skaergaard magma pursued its course to high-iron differentiates just as indicated by the "dry" silicate systems because it was dry. Kennedy (1955) has stressed the importance of oxidation state, believing that "Basalts with high ratio of FeO/Fe_2O_3 will differentiate toward a ferrogabbro as iron is concentrated in the residual liquid, thus following Fenner's trend of differentiation. Basalts with low FeO/Fe_2O_3 will differentiate toward a diorite and granite with silica and alkalis concentrated in the residual liquid, thus following Bowen's trend."

Recent laboratory research on iron oxide systems (Muan, 1955, 1958; Muan and Osborn, 1956) has shown the importance of the *constancy* of oxygen partial pressure in determining the direction of change of composition of liquid during crystallization. Two fundamentally different courses of crystallization are possible depending on whether the total composition of the mixture remains constant during crystallization or the oxygen partial pressure remains constant. The actual FeO/Fe_2O_3 ratio is of secondary importance. These systems are of course much simpler than a basaltic magma, but the same principles must apply. Furthermore, the system $MgO–FeO–Fe_2O_3–SiO_2$ (Muan and Osborn, 1956) contains the ferromagnesian components, and certainly crystallization in this system must be a reliable guide to understanding the earlier stages of crystallization of a basalt. To the classic work of Bowen and Schairer on the system $MgO–FeO–SiO_2$ which went so far in explaining crystallization processes in a basalt, we have added Fe_2O_3 which permits estimation of the effect on paths of crystallization of various oxygen partial pressure conditions.

There no doubt is more than one way to produce an andesite or a granite, and many factors are involved in the evolution of the igneous rocks. The effect of the rate of change and direction of change of oxygen partial pressure during fractional crystallization appears to be a critical factor. An explanation of this factor and its role in the crystallization and differentiation of basaltic magma will be attempted by first illustrating principles as they apply to the simpler systems $FeO–Fe_2O_3–SiO_2$ and $MgO–FeO–Fe_2O_3–SiO_2$. Basalts and related magmas will then be examined briefly to see if the observed relations in the simpler systems may not apply to basalts and possibly give another important clue to the manner of derivation of magmas.

CRYSTALLIZATION AT CONSTANT TOTAL COMPOSITION VERSUS CRYSTALLIZATION AT CONSTANT OXYGEN PARTIAL PRESSURE

The nature of the effect of the constancy of oxygen partial pressure on the course of crystallization in an iron oxide system has been discussed in recent contributions by Muan (1955, 1958), and in a paper by Muan and Osborn (1956). There are two fundamentally different ways in which the liquid and

crystalline phases may change composition during cooling. One type of crystallization path is followed if the total composition of a mixture remains constant during crystallization, as in the usual silicate system where valence change does not occur to a significant extent. The other type prevails if p_{O_2}[1] remains constant, and during crystallization of this type a change in total composition of the mixture must occur if iron oxide is a constituent. Let us illustrate this concept by describing crystallization of certain mixtures in the two systems, FeO–Fe_2O_3–SiO_2 and MgO–FeO–Fe_2O_3–SiO_2, selecting mixtures where crystallization and composition relations bear a similarity to those of a basaltic magma.

Crystallization in the System FeO–Fe_2O_3–SiO_2.—In figures 1 and 2 are reproduced two of Muan's phase diagrams for the system FeO–Fe_2O_3–SiO_2 (Muan, 1955). Figure 1 shows the primary phase fields and liquidus isotherms. From figure 2 can be read the p_{O_2} in equilibrium with condensed phases at liquidus temperatures. For purposes of discussion of crystallization paths, a part of diagram 2 including the fayalite field is redrawn in figure 3, where a slight distortion of the shape of the fayalite field has been made in order to lessen confusion in depicting relations among certain lines and points.

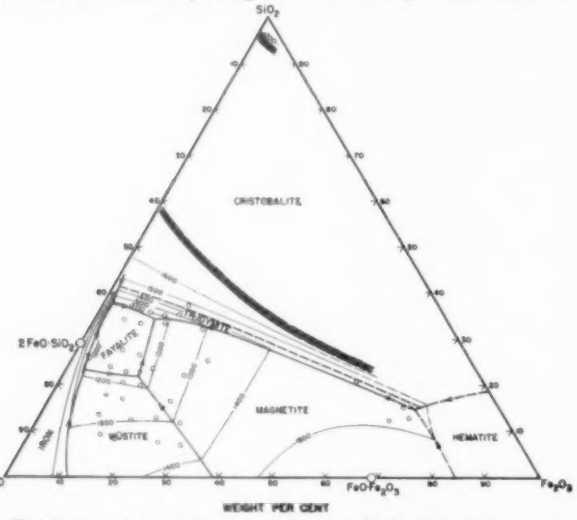

Fig. 1. Equilibrium diagram for the system FeO–Fe_2O_3–SiO_2 showing primary phase fields and liquidus isotherms, after Muan (1955).

[1] Throughout this paper the expression p_{O_2} will denote oxygen partial pressure. This term is used herein with reference to laboratory experiments carried out at a total pressure of 1 atm. as well as to magma under confining pressures of up to thousands of pounds per square inch. At low total pressures p_{O_2} represents closely the true escaping tendency (fugacity) of oxygen in the system, while at higher pressures this is only a rough approximation. At the highest pressures a gas phase may not be present at all as water, oxygen and hydrogen are completely dissolved in the liquid. Under these circumstances the p_{O_2} prevailing at the limiting total pressure above which the gas phase disappeared is a rough measure of the oxygen fugacity of the system.

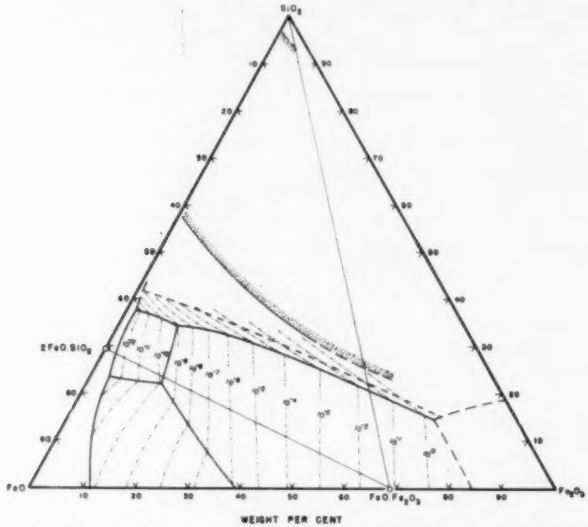

Fig. 2. Equilibrium diagram for the system FeO–Fe_2O_3–SiO_2 showing boundary curves and lines of equal O_2 pressures in atmospheres for points on the liquidus surface, after Muan (1955).

Point *a* (fig. 3) will be taken to illustrate the principal differences between crystallization at constant total composition and at constant p_{O_2}. Assume that this mixture is crystallized by continuously withdrawing heat while at all times maintaining equilibrium among the phases. Taking first the familiar case of crystallization at constant total composition, we know that as fayalite precipitates from liquid *a*, the liquid changes composition directly away from *F* toward a_1. At a_1 magnetite joins fayalite in crystallizing from the liquid, causing the latter to change its course abruptly and to follow down the boundary curve to the eutectic point *E*. At *E* tridymite, magnetite and fayalite crystallize together as liquid *E* disappears at constant temperature. Thus the final liquid has the composition of *E*, and the crystalline aggregate, of total composition *a*, is composed of fayalite, magnetite, and tridymite.

If p_{O_2} is maintained constant during crystallization rather than total composition of the mixture, then the liquid must follow down an oxygen isobar on the liquidus surface. Point *a* has a p_{O_2} of 10^{-11} at liquidus temperature. As fayalite crystallizes, therefore, the liquid must stay on the 10^{-11} isobar and change composition toward a_2. Meanwhile the total composition of the mixture changes along a line having a constant ratio of Si:Fe, the line a-a_3. Let us call this line the *total composition line*[2], being the locus of points representing the

[2] This line was designated as "isosilica" line by Muan (1955), as isosilica-magnesia line later in discussion of MgO–FeO–Fe_2O_3–SiO_2 system (Muan and Osborn, 1956), and still later was given the general term of "oxygen reaction line" (Muan, 1958). The term "total composition line" is suggested here as being preferable because of its self-explanatory nature. By "total composition" is meant that of the condensed phases, the phases represented in the usual silicate diagram.

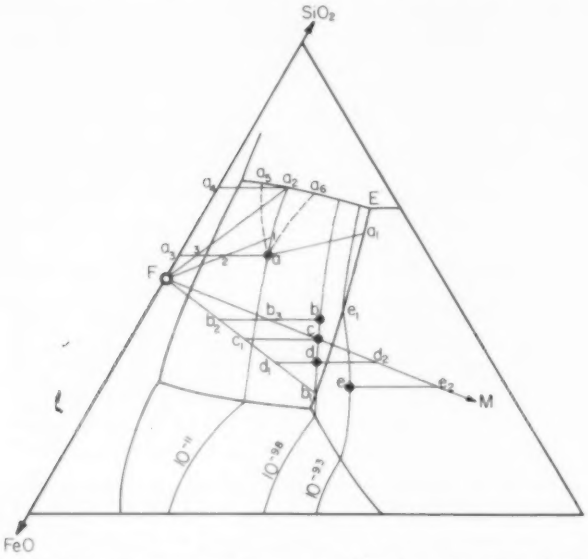

Fig. 3. Sketch to illustrate crystallization paths in the region of the fayalite field of figs. 1 and 2. F = fayalite (Fe_2SiO_4), M = magnetite (Fe_3O_4).

total composition of condensed phases making up the mixture as the mixture changes composition during crystallization. Whereas in the first type of crystallization the composition of the mixture at all times was represented by point *a*, in this second type the composition of the mixture at any stage during crystallization is represented by a point on the total composition line.

We may profitably look at the crystallization of *a* at constant p_{O_2} in a little more detail. As fayalite begins to crystallize from liquid *a* the liquid changes composition toward a_2, and the total composition of the mixture toward a_3. At the temperature of point 1, the total composition of the mixture has the composition of point 2, at the intersection of the joins *F*-1 and a-a_3, and the mixture is composed of approximately equal amounts of fayalite and liquid of composition as indicated by point 1. The mixture has lost oxygen to the atmosphere as it evidently must from the consideration that liquid 1 has approximately the same Fe_2O_3:FeO ratio as *a*, but the crystalline aggregate contains FeO and no Fe_2O_3. With continued cooling under equilibrium conditions liquid composition moves to a_2. Just as the temperature of a_2 is reached and before tridymite crystallizes, we see that the total composition of the mixture has moved along a-a_3 to 3, and the mixture now contains about 75 percent of crystals of fayalite (length a_2-3 divided by a_2-*F*). As heat is withdrawn the liquid composition must remain fixed at a_2. This is true because the liquid cannot move off the 10^{-11} oxygen isobar, and a_2 is the lowest liquidus temperature on this isobar. Fayalite and tridymite coprecipitate in the proportions as given by the point a_4, where a_2-a_4 is the total composition line through a_2,

causing the total composition of the mixture to move from 3 to a_3 and the composition of the crystalline aggregate from F to a_3.

We note that the equilibrium crystallization paths liquid a follows are very different depending on whether total composition or p_{O_2} remains constant. In the former the final liquid has composition E and the crystalline aggregate is composed of a mixture of fayalite, magnetite and tridymite. In the latter the final liquid has composition a_2, and no magnetite is present in the final crystalline body. During crystallization of the second type, oxygen has been continuously removed from the mixture. Fractional crystallization has not been considered here for neither solid solution nor incongruent melting is involved and hence the final liquid has the same composition whether or not crystals are separated from the mixture at any stage.

In the above examples the two conditions were considered which are readily definable and of most use in a discussion of crystallization paths. It is evident that an infinite variety of crystallization paths are possible if neither the total composition nor the p_{O_2} is maintained constant, just as we have the two concepts in a solid solution system of perfect equilibrium and perfect fractional crystallization, with an actual mixture following a path lying somewhere in between. The condition of total composition remaining constant is approximately realized during crystallization of mixtures in the system MgO–FeO–SiO_2, for example, because the Fe_2O_3 content of all condensed phases is kept very low. Bowen and Schairer treated the crystallization of mixtures in this system as if total composition remained constant. The condition of constant p_{O_2} is approximately realized if a sufficiently large volume of a gas is present having a constant p_{O_2}. An example of this is the laboratory study of iron oxide systems in an air atmosphere, with $p_{O_2} = 0.21$ atm.

If during crystallization of liquid a the p_{O_2} is caused to drop below 10^{-11}, the liquid may follow a course such as a-a_5. This could happen for example if the atmosphere were a mixture of H_2 and CO_2 in a constant proportion, where with decreasing temperature the p_{O_2} decreases. On the other hand the liquid might follow a path such as a-a_6 if the atmosphere is unable to accept oxygen from the crystalline mixture without the p_{O_2} rising somewhat.

As mixture a crystallized at constant p_{O_2}, the oxygen content continuously decreased. For other mixtures in the FeO–Fe_2O_3–SiO_2 system oxygen content may increase, or it may increase at one stage and decrease at another with either a net gain or loss. To illustrate, let us look briefly at mixtures b, c, d, and e, and the manner in which crystallization is carried out at constant p_{O_2}. We will assume continuous withdrawal of heat from the mixture, starting at its liquidus temperature and maintaining equilibrium among all phases. Mixtures b, c, and d all lie on the $10^{-9.8}$ isobar. Hence in each case the liquid moves along this isobar to b_l as fayalite crystallizes. At b_l temperature remains constant while fayalite and magnetite simultaneously crystallize until the liquid disappears. The final crystalline aggregate being a mixture of fayalite and magnetite has therefore a composition represented by a point on the fayalite-magnetite join (F-M, fig. 3). The final crystalline aggregate composition point must also lie on the total composition line for the mixture. Further, just as the

liquid reaches b_1, and magnetite is on the verge of crystallizing, the crystalline aggregate has the composition *F*. This requires that the total composition of each mixture at this state be represented by a point on b_1-*F*. In the case of *b*, therefore, its total composition changes from *b* to b_2 as the liquid changes from *b* to b_1, and then as the liquid crystallizes completely at b_1, the total composition moves back along b_2-*b* to b_3. The mixture has thus lost oxygen to the atmosphere as composition of the condensed phases moved from *b* to b_2, but then regained about half of this loss as the total composition point moved back to b_3.

Mixture *c*, lying on the fayalite-magnetite join, has its composition changed to c_1 and then back to *c* with no net gain or loss of oxygen, or in other words the crystalline mixture *c* at a temperature infinitesimally below that of b_1 has an Fe_2O_3:FeO ratio identical to that of liquid *c* at its liquidus temperature. The total composition of mixture *d* as it crystallizes at constant p_{O_2} changes to d_1, then back through *d* to d_2, with a net gain of oxygen. Mixture *e* in the magnetite field only gains oxygen during crystallization at constant p_{O_2}, for as the liquid moves to e_1 and disappears, composition of the condensed phases moves continuously along the total composition line from *e* to e_2.

Crystallization in the System MgO–FeO–Fe_2O_3–SiO_2

In adding MgO to the iron oxide-silica system a far more complex set of relations is obtained—still simple as compared with natural magma systems, but very difficult to portray and describe quantitatively and in detail. By sketching the system as a tetrahedron with one oxide at each apex certain relations and crystallization phenomena can be shown, at least in a qualitative way, while description of some features is best made by the use of surfaces and planes cutting through the tetrahedron.

Some of the general relations for the system MgO–FeO–Fe_2O_3–SiO_2 are shown in the tetrahedron of figure 4, after Muan and Osborn (1956). In this tetrahedron the front face has been removed so that we look inside toward the SiO_2 apex. Phase relations at liquidus temperatures are sketched on the three faces, and in addition two sets of lines of special interest to this discussion are seen passing through the tetrahedron. One set consists of univariant lines passing from the left face to the quaternary invariant point at which olivine, pyroxene, tridymite and magnesioferrite are in equilibrium with liquid, and then continuing as a single line to the fayalite-magnetite-tridymite eutectic in the right face. The pyroxene primary phase volume can be seen as a narrow wedge pinching out near the right face, bounded on the front by the olivine volume, on the top by the magnesioferrite volume, and on the back by the tridymite volume.

The second set of lines referred to above can be seen as a triangular plane on which boundary curves are sketched. The plane extends from the MgO-SiO_2 sideline to the point marked FeO·Fe_2O_3. When mixtures in the quaternary system are studied in an air atmosphere, liquids at liquidus temperatures have compositions which lie in the general neighborhood of this plane. The phase relations which are drawn on this plane are those existing on a curved surface representing liquid compositions in an air atmosphere, projected on to this plane. Treating the curved $p_{O_2} = 0.21$ atm. surface as a plane greatly

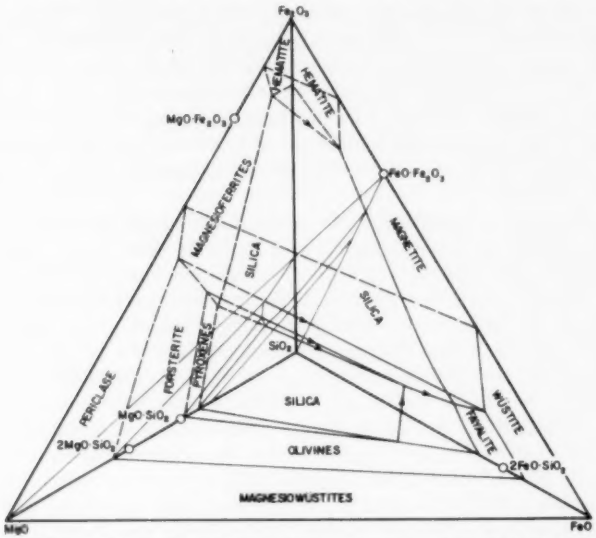

Fig. 4. Diagram illustrating phase relations in the system MgO–FeO–Fe_2O_3–SiO_2, after Muan and Osborn (1956). Sketched in light lines is the interior triangular join MgO–$FeO \cdot Fe_2O_3$–SiO_2 on which boundary curves are shown, and in heavier lines are indicated positions of quaternary univariant lines within the tetrahedron. Arrows on the lines indicate direction of decreasing temperature.

facilitates the depiction of general relations, but the distortion must be kept in mind, as will be discussed later.

A most significant difference between crystallization phenomena in this tetrahedron (fig. 4) from those in the triangle (fig. 1) arises from presence in the tetrahedron of extensive solid solution and of incongruent melting of pyroxenes at certain liquid compositions and partial pressure of oxygen conditions. Crystallization paths are not only different depending on the manner of change of p_{O_2}, as in the system FeO–Fe_2O_3–SiO_2, but now the added complication of fractional crystallization is highly important. We will distinguish for purposes of discussion the following four types of crystallization paths:

(1) Equilibrium crystallization at constant total composition,

(2) Fractional crystallization at constant total composition,

(3) Equilibrium crystallization at constant p_{O_2}, and

(4) Fractional crystallization at constant p_{O_2}.

The first two types are those ordinarily treated when considering silicate systems, for in the usual system being described the condition that total composition remains constant is approximated. Where iron oxides are present, if total composition remains constant p_{O_2} must regularly change during crystallization. On the other hand, in types (3) and (4) p_{O_2} is held constant. This latter condition is one which can be readily treated both experimentally and descriptively and hence is selected for discussion. But it must be borne in mind that there

is every gradation between types (1) and (3) and between (2) and (4), just as in figure 3 we can visualize an infinite series of crystallization paths of the type a-a_6 lying between a-a_1-E and a-a_2. Furthermore, types (3) and (4) are not the "end" or extreme situations, but rather they represent a particular or "critical" condition, like curve a-a_2 of figure 3, with a series of crystallization paths even farther removed from those of types (1) and (2) being possible, in the way that there exists to the left of a-a_2 in figure 3 a series of curves like a-a_5.

Equilibrium crystallization at constant total composition.—Only mention need be made of this case inasmuch as it has been discussed in some detail in a preceding paper (Muan and Osborn, 1956). In figure 5, after Muan and Osborn (1956), are shown representative sets of conjugation lines joining the composition of liquids on quaternary univariant lines with the composition of crystalline phases in equilibrium with these liquids. If a mixture has a composition within the volume bounded by the olivine join ($2MgO \cdot SiO_2$-$2FeO \cdot SiO_2$), the spinel join ($MgO \cdot Fe_2O_3$-$FeO \cdot Fe_2O_3$) and the silica apex, the first crystal to separate on cooling the liquid under equilibrium conditions will be an olivine, a pyroxene, a magnesioferrite or tridymite (or cristobalite). If silica is the primary phase, the liquid changes along a straight line away from the SiO_2 apex, whereas if one of the other three is first to crystallize the liquid composition change is along a curved path with the composition of the solid solution continuously changing along its composition join. The liquid in any case will eventually reach one of the univariant lines passing through the tetrahedron and will soon disappear. Crystallization is very similar in nature to that appearing on the base of the tetrahedron, and described in detail by Bowen and Schairer (1935) in their treatise on the system MgO–FeO–SiO_2. The chief difference lies in the higher ferric oxide content of the liquids and in the presence of magnesioferrite as a phase.

Fractional crystallization at constant total composition.—Referring again to figure 5, fractional crystallization carried out under the condition that total composition of a mixture is kept constant is naturally somewhat similar to the preceding case with the main differences being: (a) the liquid does not disappear shortly after it reaches one of the univariant lines, and (b) p_{O_2} decreases significantly during the process. With perfect fractional crystallization all liquids after reaching a univariant line move continuously to the right on this line with decreasing temperature, past the point g and on toward the fayalite-magnetite-tridymite eutectic in the right face. As this happens the composition of each of the solid solution crystals, olivine, pyroxene, and magnesioferrite moves also to the right approaching the high iron oxide end member of each series. The amount of drop in p_{O_2} during the fractional crystallization depends of course on the initial and final liquid compositions. With extreme fractional crystallization, p_{O_2} approaches the value of 10^{-9} atm. at the composition of the fayalite-magnetite-tridymite eutectic (see fig. 2).

This direction of change of liquid with fractional crystallization at constant total composition is very similar to that for the system MgO–FeO–SiO_2. *Extreme fractional crystallization of any mixture at constant total composition can only produce a high iron differentiate.* It is very important for this discus-

sion and for its implications relative to the crystallization of basaltic magma to note that the Fe_2O_3:FeO ratio of the original mixture is unimportant as regards the later course of fractional crystallization. If the liquid has a very high Fe_2O_3:FeO ratio, magnesioferrite crystallizes first and the liquid approaches the univariant curves from above. If the ratio is low, the liquid during fractionation approaches these univariant curves from below. Always the liquid moves down these curves to the right increasing in iron oxide content and finally disappearing at some point along one of the lines, the point being determined by the degree to which perfect fractionation has been approached.

Equilibrium crystallization at constant p_{O_2}.—In the preceding discussion of crystallization at constant p_{O_2} in the system FeO–Fe_2O_3–SiO_2, we noted that if p_{O_2} is maintained constant, the liquid during crystallization must follow an oxygen isobar down the liquidus surface, disappearing at the point on the isobar of lowest liquidus temperature. In the quaternary system MgO–FeO–Fe_2O_3–SiO_2 this same principle applies, but now with the addition of one dimension the lines of figure 2 become surfaces in the tetrahedron. During crystallization the liquid must remain on the surface corresponding to the particular p_{O_2} which is being held constant, while the total composition of the condensed phases changes along a total composition line as oxygen is being either added to or subtracted from the mixture. The liquid moves down the isobaric surface in the general direction of the lowest liquidus temperature point, but in this quaternary system having solid solutions, with equilibrium crystallization it may not reach the lowest point before disappearing.

As a typical example of equilibrium crystallization at constant p_{O_2} we will

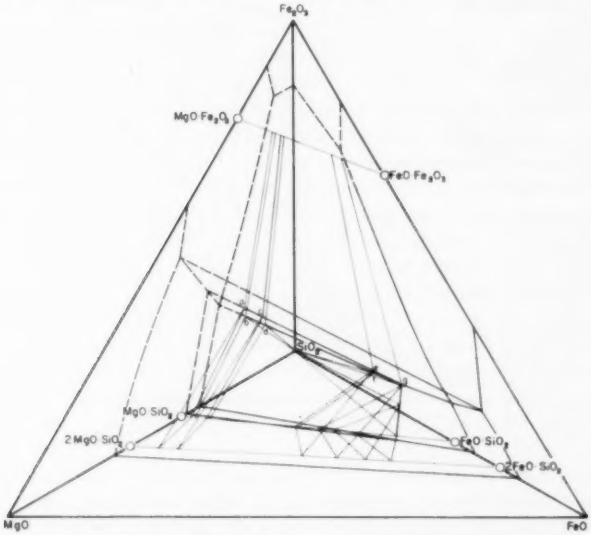

Fig. 5. Tetrahedral diagram for the system MgO–FeO–Fe_2O_3–SiO_2 showing some composition relations among liquid and crystalline phases in equilibrium, after Muan and Osborn (1956).

take the case of liquids crystallizing in an air atmosphere where $p_{O_2} = 0.21$ atm. Data have been obtained for this surface (Muan and Osborn, 1956). The liquidus phase relations for the air atmosphere surface are shown projected onto the MgO-$FeO \cdot Fe_2O_3$-SiO_2 plane in figures 4 and 7. For the present let us consider that the isobaric surface and this plane are identical. This approach greatly simplifies construction and description of general relations. The manner in which these are modified where the actual curved surface is used instead of the plane will be taken up later.

In figure 6 two surfaces within the tetrahedron are shown intersecting. One is the triangular join, $2MgO \cdot SiO_2$-$FeO \cdot Fe_2O_3$-SiO_2, (Fo-S-M in fig. 6), the part of the MgO-$FeO \cdot Fe_2O_3$-SiO_2 plane of special interest in this discussion. In its central section, this plane passes behind the other surface. The other is a complex surface of three intersecting planes whose corners, *c'*, *d'*, *S*, *d''*, *c''*, and *c'''*, represent the composition of crystalline phases in equilibrium with liquids *c* and *d* on the Fo-S-M plane. Liquids *c* and *d* and the crystalline compositions *c'*, *d'*, *c''*, *c'''* and *d''* are the same as points shown in figure 5, although they have been shifted slightly in figure 6 in order to show relations better.

Let us start with a mixture whose composition is represented by a point on the Fo-S-M plane. With crystallization at constant p_{O_2} the liquid must stay on the Fo-S-M plane, assuming as stated above that this is the isobaric surface where $p_{O_2} = 0.21$ atm. On the other hand, the crystalline aggregate resulting from equilibrium crystallization of the mixture must have a composition lying

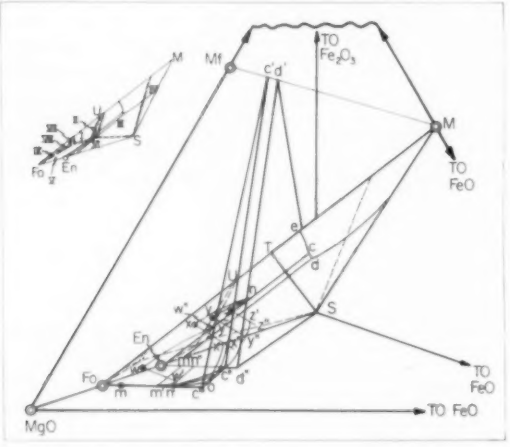

Fig. 6. Sketch of a part of the tetrahedron MgO–FeO–Fe_2O_3–SiO_2 to illustrate crystallization paths at constant p_{O_2}. The plane Fo-S-M, part of the plane MgO–$FeO \cdot Fe_2O_3$–SiO_2 of fig. 4, is shown intersected by the crystal composition surface. Lines are drawn representing paths followed by the liquid, the crystalline aggregate and the total composition of the mixture as they change composition during crystallization of mixtures *w*, *x*, *y* and *z* at constant p_{O_2}. Fo = forsterite ($2MgO \cdot SiO_2$), En = enstatite ($MgO \cdot SiO_2$), S = SiO_2, Mf = magnesioferrite ($MgO \cdot Fe_2O_3$), M = magnetite ($FeO \cdot Fe_2O_3$).

on the *crystal composition surface*. This surface consists of two principal parts: a basal area Fo-*c'''*-*c''*-*d''*-*S*, and the approximately vertical surface mentioned above, *c'*-*d'*-*S*-*d''*-*c''*-*c'''*. The total composition of the mixture must move during crystallization along a total composition line from the Fo-S-M plane to the crystal composition surface. This requires a net gain or loss in oxygen. Along the line of intersection of the plane Fo-S-M and the crystal composition surface (*ST* fig. 6), mixtures crystallize without net gain or less, just as mixture *c*, along the FM join in figure 3. If a mixture must move along its total composition line to the right during crystallization in order to reach the crystal composition surface, as is the case in the lower part of the diagram (area Fo-S-T) oxygen is lost; whereas if the total composition of the mixture moves to the left, as it will for the area *T*-*S*-*M*, oxygen is added. In either case the total composition line extends from the point representing the composition of the mixture at liquidus temperatures toward or away from the oxygen apex of the system Mg–Fe–Si–O.

On the Fo-S-M plane (figs. 6 and 8) the field for pyroxene solid solutions is a narrow, central area extending from the Fo-S edge to the boundary *c*-*d*. Point *c* is the reaction point at which pyroxene, olivine and magnesioferrite are in equilibrium, representing the composition of liquid in equilibrium with these three phases. Point *d* is a eutectic-like point at which pyroxene, tridymite and magnesioferrite are in equilibrium with liquid *d*. Neither *c* nor *d* is an invariant point, but rather a piercing point where a quaternary univariant line intersects this plane. Inasmuch as the oxygen pressure is fixed, however, no degrees of freedom are left when the three crystalline phases and liquid are in equilibrium, and hence *c* and *d* can be treated just like a ternary peritectic and eutectic point respectively.

Dashed lines on the Fo-S-M plane divide it into nine areas on the basis of the assemblage present when the mixture is entirely crystalline. These areas are labeled with Roman numerals in the sketch shown in the upper left part of figure 6. Under equilibrium conditions the crystalline assemblages at temperatures just below the solidus for mixtures whose compositions lie in the various areas are as follows: Area I, olivine, pyroxene and magnesioferrite; area II, pyroxene and magnesioferrite; area III, pyroxene, silica and magnesioferrite; area IV, silica and magnesioferrite; area V, olivine and pyroxene; area VI, pyroxene and silica; area VII, olivine and magnesioferrite; area VIII, olivine, magnesioferrite and magnesiowustite; area IX, olivine and magnesiowustite.

Equilibrium paths of crystallization for mixtures on the isobaric plane Fo-S-M can be sketched and visualized without much difficulty if one can sense what the writer has attempted to show in this perspective drawing (fig. 6). Points have been shifted slightly from true positions, without changing their significance, in order to avoid as far as seems possible a serious confusion of lines. This distortion is apparent for example in the slope of the total composition lines which should approximately parallel the Fe_2O_3-FeO side line, but in this figure are shown with a much lower slope. To illustrate equilibrium crystallization at constant P_{O_2}, the path of crystallization of a few typical mixtures will be described.

Let us take first mixture *w* which lies in area V and must therefore

crystallize to a mixture of pyroxene and olivine. As heat is withdrawn from liquid w at its liquidus temperature, olivine of composition m begins to precipitate. Three different but related composition trends must now be noted. The composition of the mixture begins to change along the total composition line w-w', losing oxygen. The composition of the olivine changes along the olivine join from m toward m'. The composition of the liquid follows a curved path in the Fo-S-M plane toward the pyroxene-olivine boundary curve. When the liquid reaches the boundary curve (point w''), the olivine has the composition m', and pyroxene crystals of composition m'' begin to form. The lines m'-m'' and n'-n'' are conjugation lines of the type joining the composition of olivine and pyroxene in equilibrium with one another and a liquid whose composition lies along the pyroxene-olivine boundary curve in the Fo-S-M plane. With the liquid at w'' and the crystalline aggregate having the composition m', the total composition of the mixture is at a point on w-w' where w-w' is intersected by a line joining m' and w''. The proportions of liquid and of olivine crystals are given by the relative lengths of the portions of the line m'-w'' on either side of w-w'. The mixture is approximately 85 percent crystals of olivine m' and 15 percent liquid w''. With further equilibrium cooling, the liquid moves down the boundary curve from w'' to n, disappearing completely as its composition reaches n. As the liquid is moving from w'' to n, olivine reacts with the liquid to partly disappear while at the same time changing composition from m' to n'. Simultaneously pyroxene crystallizes, changing composition from m'' to n''. The composition of the mixture changes to w', a completely crystalline mixture of olivine n' and pyroxene n'' in the proportions as given by the lengths w'-n'' and w'-n' respectively. The crystalline aggregate has thus changed its composition from m to m' and thence along the curved path to w', while the total composition of the mixture moved from w to w' and the liquid moved from w to w'' to n.

In the case of mixture w the total composition line intersected the base of the tetrahedron before reaching the crystal composition surfaces extending from the base toward c' and d'. Therefore no magnesioferrite formed. We will next consider mixtures x, y and z from which magnesioferrite crystallizes.

Mixture x lies in area I of the insert in figure 6. Its total composition line therefore intersects the crystal composition surface in the plane c'''-c''-c', or in other words the final crystalline aggregate will be composed of olivine c''', pyroxene c'' and magnesioferrite c'. Lying in the olivine field, mixture x precipitates olivine as the liquid changes composition along the curved path to n. At n, olivine of composition n' is joined by pyroxene of composition n'', and the liquid moves down the boundary curve to the reaction point c as olivine continuously dissolves and pyroxene crystallizes. When the liquid has reached c, magnesioferrite of composition c' and pyroxene of composition c'' crystallize while olivine of composition c''' continues to dissolve. The composition of all phases and the temperature of the mixture remain constant until the liquid has disappeared. During this crystallization the total composition of the mixture changes along the line x-x''. The point x'', lying in the c-c''-c''' plane (this plane is not sketched), is the composition reached by the mixture x just as the liquid reaches c; then as liquid c crystallizes, the composition of the mixture

moves back along its total composition line, x-x'', to x' in the plane c'-c''-c'''. In other words, oxygen is lost by the condensed phases continuously until magnesioferrite begins to crystallize, at which point the mixture begins to increase in oxygen content. The constitution of the crystalline aggregate at any stage as well as the proportion of crystals and liquid can be estimated readily from the diagram, for curves are shown for composition of the crystals as well as for liquid and mixture. The composition of the crystalline aggregate during cooling follows first the olivine join to n', then the curve n'-o as olivine and pyroxene are in equilibrium, and finally the curve o-x' along the surface c'''-c''-c'. The crystalline aggregate composition reaches x' just as the total composition of the mixture reaches this point, and this coincides with the disappearance of liquid c.

Mixture y crystallizes in a manner similar to that just described for x. Point y however is located on the border between areas I and II. It will therefore crystallize entirely to pyroxene and magnesioferrite. As y crystallizes under equilibrium conditions olivine again is the first phase to separate causing the liquid to move along the curved path to n. Subsequent crystallization differs from that of mixture x in that all of the olivine disappears simultaneously with the disappearance of liquid c. The total composition of mixture y changes to y'' and then back to y'. The points y'' and y' are analogous to x'' and x', lying in the c-c''-c''' and c'-c''-c''' planes respectively. The composition of the crystalline aggregate follows along the olivine join to n', then along the curved path as shown in Fig. 6 intersecting c'''-c'' at a point between o and c'', and thence up along the crystal composition surface to y' which lies on the pyroxene-magnesioferrite conjugation line, c''-c'. The final crystalline aggregate is therefore composed of pyroxene c'' and magnesioferrite of composition c'. The proportion of pyroxene is given by the ratio y'-c':c''-c'.

The point z is an example of a mixture in area III. Like x and y, olivine is the primary phase, but in z olivine must completely dissolve before disappearance of liquid. The point z is located in such a position that the liquid reaches c just as the last of the olivine disappears. On reaching c, therefore, the liquid does not pause as heat is withdrawn but continues to change composition, proceeding down c-d to d where tridymite, pyroxene d'' and magnesioferrite d' crystallize together until the liquid is gone. The curve for the composition of the crystalline aggregate therefore moves from n' exactly to c'' without intersecting c'''-c'' or c''-n''. From c'' this curve giving the composition of the crystalline part of the mixture continues upward along the pyroxene-magnesioferrite crystal composition surface (c''-d''-d'-c') simultaneously with the liquid moving from c to d. As the liquid crystallizes at the constant temperature of d, the crystalline aggregate composition line moves into and along the pyroxene-silica-magnesioferrite crystal composition surface to z'. The total composition of the mixture has moved from z' to z'' and back to z'. The point z'' is the intersection of the line c-c'' with z-z'', while the point z' lies in the plane d'-d''-S.

If another mixture were taken between z and c, olivine would disappear before the liquid reaches c. The liquid would then cross the pyroxene field either to the pyroxene-silica boundary curve or to the pyroxene-magnesiofer-

rite boundary curve, the path taken depending on the composition of the mixture, and thence down this curve to *d*.

Other points of interest might be brought out by consideration of mixtures in other areas, but it is hoped that this brief discussion will orient the reader with respect to the types of crystallization paths which are possible and the general nature of crystallization under equilibrium conditions when p_{O_2} remains constant.

Before leaving figure 6 it may be instructive to make a type of comparison between equilibrium crystallization at constant p_{O_2}, as just discussed, with equilibrium crystallization at constant total composition which was taken up earlier. Liquid *c* is in equilibrium with crystals *c'*, *c''*, and *c'''*. Liquid *d* is in equilibrium with crystals *d'*, *d''* and *S*. Therefore under conditions of *constant total composition*, mixtures lying on the surface *c'-c''-c'''* will crystallize with the final liquid having the composition *c*, and mixtures with compositions on the surface *d'-d''-S* will crystallize with the final liquid having the composition *d*. For these two sets of mixtures, therefore, the final liquids developed during equilibrium crystallization at constant total composition are the same as the two final liquids for mixtures in areas I and III respectively where the equilibrium crystallization is at *constant* p_{O_2}. An opportunity is thus afforded by this diagram in conjunction with figures 4 and 5, to compare directly the differing routes followed by the liquid in arriving at *c* and at *d* during crystallization under these two types of conditions. The path of the liquid in a mixture crystallizing at constant total composition reaches the quaternary univariant line at a higher temperature point than would the liquid of the same mixture crystallizing at constant p_{O_2}. After reaching the univariant line a liquid in the process of crystallization at constant total composition continues its movement down this line. With constant p_{O_2} crystallization the liquid moves to a quaternary univariant line but there stops or leaves the line but does not proceed down along the line.

The diagram of figure 6 is schematic as mentioned earlier, for the constant p_{O_2} surface Fo-S-M is drawn as a plane. The constant p_{O_2} surface in reality is decidedly bowed, being convex toward the FeO apex of the tetrahedron. If the surface were a plane the Fe_2O_3:FeO ratios of liquids on the plane would be constant. Actually these ratios are low toward the Fo apex of the surface, increasing almost regularly in moving along the Fo-M join to M. This relation can be seen in the diagram reproduced as figure 7, after Muan and Osborn (1956). From this diagram can be read the actual liquid compositions and temperatures of the liquidus surface for all mixtures in the system MgO–FeO–Fe_2O_3–SiO_2 at the constant p_{O_2} of 0.21 atm. It will be noted that in passing from left to right across the olivine, pyroxene and magnesioferrite fields the Fe_2O_3/FeO ratio increases. Therefore, upon crystallization of mixtures *x*, *y* and *z* (fig. 6), as just described, the Fe_2O_3:FeO ratio of the liquid will continuously increase as it changes composition. Liquid *c* has the composition[3]: 19MgO, 41FeO_x[4], 40SiO_2 with an Fe_2O_3:FeO ratio (wt.%) of 1.83. It is in equilibrium at 1374° with olivine having the composition 87Mg_2SiO_4,

[3] Compositions are in wt. percent.

[4] The term FeO_x is used to denote the sum, FeO + Fe_2O_3.

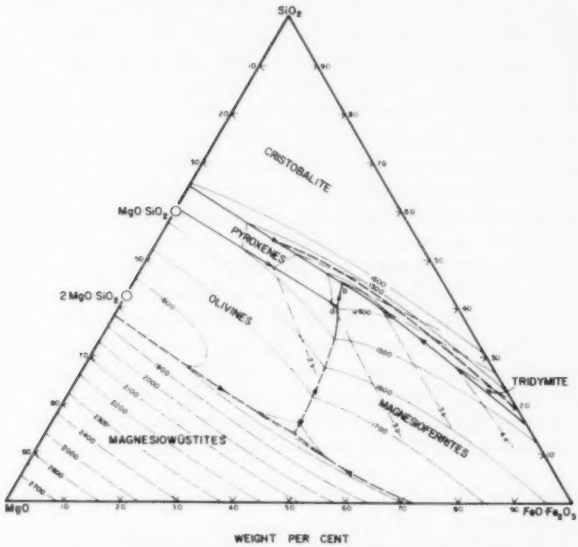

Fig. 7. Diagram to illustrate phase relations on the surface of constant $p_{O_2} = 0.21$ atm. in the system MgO–FeO–Fe_2O_3–SiO_2, after Muan and Osborn (1956). For the sake of simplicity the surface is pictured as a ternary system with MgO, $FeO \cdot Fe_2O_3$ and SiO_2 as components. Dash-triple dot lines are curves approximately passing through points of equal Fe_2O_3/FeO ratios at liquidus temperatures.

$13Fe_2SiO_4$, pyroxene $91MgSiO_3$, $9FeSiO_3$, and magnesioferrite $65MgFe_2O_4$, $35FeFe_2O_4$. Point *d* has the composition: 16MgO, $39FeO_x$, $45SiO_2$, with an Fe_2O_3:FeO ratio of 2.2, and is in equilibrium at 1367° with tridymite, pyroxene and magnesioferrite, the latter two having slightly higher FeO:MgO ratios than those in equilibrium with liquid *c*.

As a consequence of the curvature of the $p_{O_2} = 0.21$ atm. surface, two important lines as shown in figure 6 have somewhat different dispositions when drawn taking the actual shape of the Fo-S-M surface into consideration. These are the line of intersection of the two surfaces, *S-T* (fig. 6), and the line extending from *En* to *U* separating areas V and I from VI and II. On figure 8, the same projection as figure 7, are shown the lines *S-T* and the dashed lines outlining the crystallization areas.[5] Roman numerals have the same significance as in figure 6. Actual relations as they exist on the Fo-S-M surface can be read from figure 8, combined with figure 7 for Fe_2O_3/FeO ratio of liquids and liquidus temperatures. Composition of the olivine, pyroxene and magnesioferrite phases however cannot be read from these diagrams; but they can be estimated from general considerations knowing the composition of these crystalline phases in equilibrium with liquid *c*, as given above.

[5] In figure 8 the dashed lines and the line ST have been drawn as straight lines, neglecting the slight curvature—an approximation sufficient for purposes of this discussion.

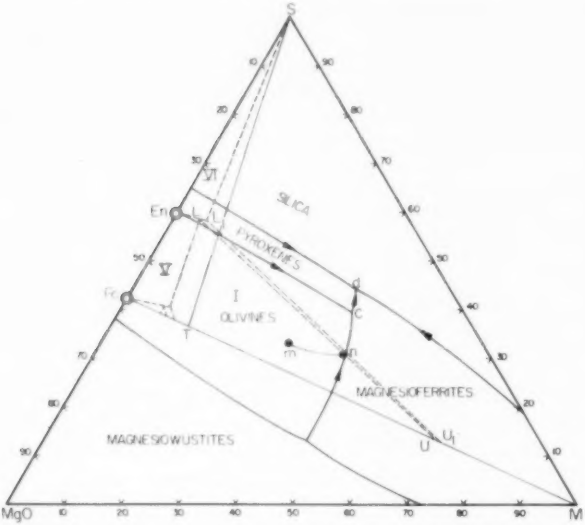

Fig. 8. Sketch of the $p_{O_2} = 0.21$ atm. surface for further illustration of courses of crystallization at constant p_{O_2}.

The line *S-T* in figure 8 is shifted notably toward the *Fo-S* side line as compared with its distorted position in figure 6. Inasmuch as all mixtures lying to the right of this line have a net increase in oxygen during crystallization at constant p_{O_2}, mixtures over most of the area of the olivine and pyroxene fields have this characteristic. The line *En-L-U* is rotated from its position in figure 6, so that in figure 8 it crosses the olivine-magnesioferrite boundary curve. Mixtures within the narrow zone L-U-U_1-L_1 crystallize at equilibrium entirely to pyroxene and magnesioferrite. This zone crosses the olivine field and hence olivine is the first phase to crystallize, but all olivine which forms must react with the liquid and disappear if equilibrium is maintained. Mixtures richer in silica than the line L_1-U_1 crystallize at equilibrium to tridymite, pyroxene and magnesioferrite at the temperature of *d*. If the composition of a crystallizing mixture lies below the line *L-U* (area I), the liquid moves to *c* and disappears at this point with olivine still present along with pyroxene and magnesioferrite. If the mixture lies on *En-L*, liquid and olivine disappear simultaneously while the liquid is on the boundary curve and before it reaches *c*, leaving a crystalline aggregate composed only of crystals of pyroxene. With a mixture on *L-U*, the last of the liquid disappears at *c*, just as the last of the olivine disappears, and the crystalline aggregate is pyroxene and magnesioferrite. For a composition in the area L-U-U_1-L_1 olivine disappears before the liquid is gone, and the latter disappears at a point along the boundary curve *c-d*.

The importance of the manner of change of p_{O_2} on the olivine-pyroxene reaction is well illustrated by relations shown in the triangle Fo-M-S, occupying the upper part of figure 8. It can be seen that magnetite acts very much as

does anorthite in extending the size of the compositional area within which olivine first crystallizes but then must be later resorbed with equilibrium crystallization. Just as in the system forsterite-anorthite-silica (Andersen, 1915), so in the Fo-M-S triangle of figure 8 the compositional area within which silica occurs in the final equilibrium crystalline aggregate overlaps a significantly large section of the olivine field. In contrast with this, if crystallization occurs with falling p_{O_2} corresponding to the condition of constant total composition, the compositional region within which "excess" olivine precipitates is small and occurs only in the low iron oxide region. This can be visualized by noting from figure 4 that with crystallization at constant total composition the olivine-pyroxene relation for quaternary mixtures is similar to that for "ternary" mixtures on the base (MgO-FeO-SiO_2) where only a small corner of the olivine field lies on the silica side of the pyroxene join. It is a significant fact therefore from the standpoint of the crystallization and differentiation of basaltic magma that the manner of change of p_{O_2} affects the extent of the olivine-pyroxene reaction relation. As the rate of decrease in p_{O_2} during crystallization lessens approaching the condition of constant or of increasing p_{O_2}, the range of compositions for the olivine-pyroxene reaction increases.

Fractional crystallization at constant p_{O_2}.—Following this discussion of equilibrium crystallization at constant p_{O_2}, fractional crystallization can be treated briefly. The final liquid from the fractional crystallization of any mixture in the Fo-S-M triangle (fig. 8) has the composition *d*. With p_{O_2} constant, the liquid during crystallization must stay on the surface of constant O_2 pressure just as in equilibrium crystallization. For the surface shown in figure 8, a liquid within Fo-S-M can only move to *d* and then finally crystallize. It is important to note that fractional crystallization at constant p_{O_2} differs in a very fundamental aspect from fractional crystallization at constant total composition. In the latter with extreme fractionation the amount of liquid becomes vanishingly small. The more extreme the fractionation, the more extreme the composition of the liquid and the less there is of it. This is not the case with fractionation at constant p_{O_2} in the system MgO–FeO–Fe_2O_3–SiO_2. For mixtures analogous to basalts, that is, those that crystallize predominantly to pyroxene with magnesioferrite, fractional crystallization whether of a nominal or extreme extent causes the liquid to move to the same point, *d*. In essence, fractional crystallization serves to purge the liquid of olivine and some pyroxene and magnesioferrite crystals, but then terminates at *d* in large quantities.

If we fractionally crystallize a mixture such as *m* at the constant p_{O_2} of the surface represented by figure 8, the liquid moves to the boundary curve at *n*, and then abruptly turns to move to *c* and then to *d*. As the liquid moves from *m* to *n* with olivine separating the silica content of the liquid decreases slightly. As soon as magnesioferrite begins to crystallize, however, silica content continuously increases from 30.5 percent at *n* to 44 percent at *d*. The iron oxide content of the liquid increases rapidly from *m* to *n*, but then decreases slowly from *n* to *d*. The separation of magnesioferrite thus prevents liquids fractionating at constant p_{O_2} from increasing in iron oxide content beyond a certain

point, and causes the liquid to move in the direction of increased silica content.

Fractional crystallization at constant total composition and at constant p_{O_2} compared.—In the discussion of *equilibrium crystallization* at constant p_{O_2}, a comparison was made with equilibrium crystallization at constant total composition. Although fundamental differences exist in the two crystallization processes, the final liquid and the crystalline assemblage are not so very different. In contrast with this, *fractional crystallization* under the two sets of conditions is strikingly different, resulting in final liquids very unlike both in composition and amount.

Referring to figure 5, a liquid fractionally crystallizing at either constant total composition or constant p_{O_2} will move to the magnesioferrite surface. If olivine or pyroxene is the primary phase, then the liquid moves upward to this boundary surface, and precipitation of magnesioferrite prevents the liquid from moving any farther upward in the tetrahedron, i.e. to higher Fe_2O_3 contents. If the Fe_2O_3:FeO ratio is sufficiently high that magnesioferrite is the primary phase, the liquid will move downward to this surface. The initial Fe_2O_3:FeO ratio of a mixture has little bearing on the composition of the final liquid produced by fractional crystallization. The surface separating the primary phase volume of magnesioferrite from those of olivine and pyroxene, herein called the magnesioferrite surface, acts as a roof which liquids reach but cannot penetrate. Now if fractional crystallization is being carried out with total composition remaining constant, the liquid slides down this roof toward point *g* or beyond toward the fayalite-magnetite-silica eutectic in the right face. The final composition and amount of liquid depend on the degree to which perfect fractional crystallization has been approached, but it is clear that with the liquid moving down the magnesioferrite surface the iron content continuosly increases and the silica content decreases, and the farther the liquid goes down this roof the less there is of it. Precipitation of magnesioferrite has served as a regulator on the Fe_2O_3:FeO ratio in the liquid, preventing this from going above or below a certain amount, but as for its effect on iron oxide content of the liquid, its precipitation along with that of olivine and pyroxene has helped push the liquid to continuously higher iron oxide contents as fractional crystallization proceeded.

In contrast with this, the precipitation of magnesioferrite has a profound effect on the change in composition of the liquid where crystal fractionation is carried out at constant p_{O_2}. This is because the O_2 isobaric surface on which the liquid must remain intersects this magnesioferrite surface, and hence the fractionating liquid cannot slide down the magnesioferrite roof and continue to increase in iron content. As soon as the magnesioferrite surface is reached, the liquid must turn abruptly in the direction of silica and move along the magnesioferrite surface to the boundary with the silica phase volume. When the silica boundary is reached the liquid can go no farther. It is trapped and must now with further withdrawal of heat crystallize to an aggregate of this composition. This final liquid may be a large percentage of the original mixture, the amount depending of course on the original composition.

In figure 9 are shown curves which illustrate the difference in the direction of change of composition of the liquid as it is crystal fractionated under

the two sets of conditions. The starting mixture is point *n* of figure 8, which lies at the magnesioferrite surface in the olivine field. Plotted against silica content of the liquid is its $FeO + Fe_2O_3/FeO + Fe_2O_3 + MgO$ ratio in figure 9a, and total iron oxide in figure 9b. With *partial pressure of oxygen remaining constant*, the liquid moves to *c* and then to *d* (fig. 8). The curve *n-c-d* for these liquids derived by fractional crystallization at constant p_{O_2} rises gently and

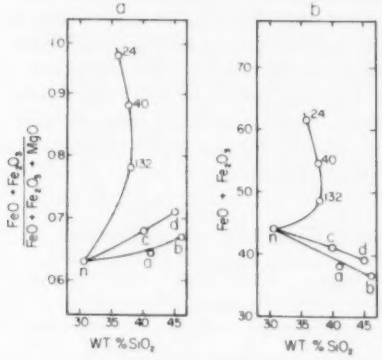

Fig. 9. Curves for comparing manner of change in composition of liquid as mixture *n* of fig. 8 is fractionally crystallized under the conditions of: (1) constant total composition (curves *n*-132-40-24), (2) constant p_{O_2} (curves *n-c-d*), (3) increasing p_{O_2} from 0.21 to 1.0 atm. (curves *n-b*).

regularly in figure 9a, and in figure 9b it falls in the same manner. With mixture *n* fractionally crystallized *at constant total composition*, the liquid does not stay on the surface of figure 8 but moves more strongly to the right through the tetrahedron (fig. 4), following down the magnesioferrite roof and intersecting the pyroxene-olivine surface at a point to the right of *c*. With perfect fractionation the liquid passes through the "reaction point" where the CO_2/H_2 mixing ratio is 132 (Muan and Osborn, 1956, fig. 7). The liquid continues on down the quaternary univariant line, and besides this "point 132", two other points which the liquid must pass through during fractionation have been located. These are eutectic-like points at constant CO_2/H_2 mixing ratios of 40 and of 24, shown in figures 8 and 9 of paper by Muan and Osborn (1956). These three composition points, which we will denote simply as points 132, 40 and 24 have compositions as shown in table 1. When these points *n*-132-40-24 are plotted in figures 9a and 9b, it is seen that curves representing change in composition of liquid during fractional crystallization at constant total composition rise steeply. They are concave to the left as a result of an initial increase and a later decrease in silica content. The initial increase in SiO_2 occurs during crystallization of olivine and magnesioferrite while the liquid moves to the pyroxene-olivine-magnesioferrite boundary curve.

To illustrate courses of crystallization at constant p_{O_2} we have used an atmosphere in which $p_{O_2} = 0.21$ atm. A surface of different p_{O_2} might have been taken. If so, a difference would be noted in the early stages of the crystalliza-

tion, especially in Fe_2O_3/FeO ratios and in composition of olivine, pyroxene and magnesioferrite crystals. It is important to note, however, that the same types of crystallization curves exist for the other surfaces of constant p_{O_2}. With either equilibrium or fractional crystallization at constant p_{O_2} the liquid has to stay on its constant p_{O_2} surface, and hence no matter how extreme the fractional crystallization, the liquid will not move down the quaternary univariant lines toward the high iron oxide contents. Thus initial Fe_2O_3/FeO ratio of a mixture has only a secondary effect on the course of crystallization. Actually, despite their high p_{O_2} as compared with that for basalts, liquids *n*, *c* and *d* (fig. 8) are not extreme as liquids for comparison with natural magmas, but have about the $FeO + Fe_2O_3/FeO + Fe_2O_3 + MgO$ ratio of basalts, andesites and dacites, respectively (figs. 9 and 11); and crystals in equilibrium with liquids *n*, *c* and *d* have compositions in the right neighborhood for crystals separating from the natural liquids.

TABLE 1

Composition of Points Shown in Figures 7, 8, 9 and 10

Point	MgO	FeO	Fe_2O_3	SiO_2
n	25.5	17.6	26.4	30.5
a	21	9.3	28.7	41
b	18	8.5	28	45.5
c	19	14.5	26.5	40
d	16	12.0	27.0	45
132	13.5	34.7	13.8	38
40	7.5	43.2	11.3	38
24	2.5	50.8	10.7	36

Crystallization under other conditions.—We have used as the two extreme conditions for comparison of fractional crystallization those of constant total composition and of constant p_{O_2}. These are two conditions which can be treated quantitatively and illustrated by relatively simple diagrams. Between the two types of crystallization paths lie an infinite number of intermediate paths. Inasmuch as p_{O_2} decreases during constant composition crystallization for mixtures in the system $MgO–FeO–Fe_2O_3–SiO_2$ resembling simplified basalts, as well as for basalts, p_{O_2} will decrease for all of these intermediate paths but at a slower rate than for the condition of constant total composition.

The oxygen partial pressure may also increase during crystallization. For natural liquids this might happen, for example, if water pressure is increasing at a sufficiently rapid rate. For the condition of increasing p_{O_2}, crystallization paths will leave the constant p_{O_2} surface moving through surfaces of increasingly higher p_{O_2}. Specifically for the case being considered here, the liquid of mixture *n*, instead of remaining on the surface $p_{O_2} = 0.21$ atm. (figs. 7 and 8), will move toward the surface $p_{O_2} = 1.0$ atm., with crystallization. In figure 10 is shown the diagram for $p_{O_2} = 1.0$ atm. with phase relations projected onto the $MgO\text{-}FeO\cdot Fe_2O_3\text{-}SiO_2$ plane. The diagram resembles very closely that of figure 7, the main differences being in lower iron oxide content of liquids at the "peritectic" and "eutectic" points (*a* and *b* of fig. 10 and also of fig. 5), and the higher Fe_2O_3/FeO ratios of the liquids. Referring to figures 4 and 5,

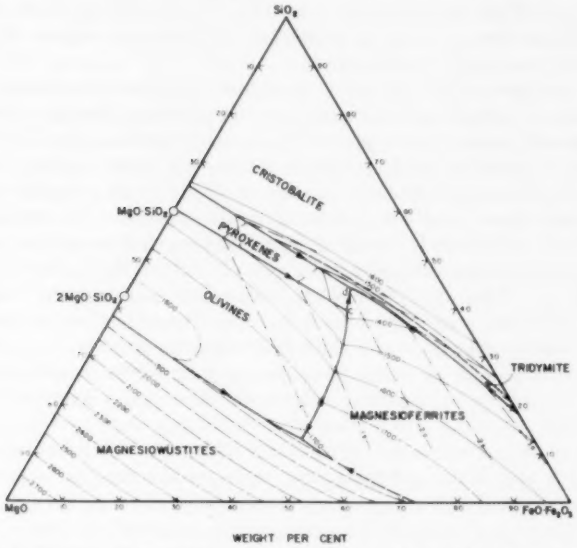

Fig. 10. Diagram to illustrate phase relations on the surface of constant p_{O_2} = 1.0 atm. in the system MgO–FeO–Fe_2O_3–SiO_2, after Muan and Osborn (1956). As in fig. 7, phase relations are shown projected onto the MgO–FeO·Fe_2O_3–SiO_2 plane. Dash-triple dot lines are curves approximately passing through points of equal Fe_2O_3/FeO ratios at liquidus temperatures.

we see that curves for composition change of liquids on fractional crystallization will intersect the quaternary univariant curves at higher points in the tetrahedron the more the p_{O_2} is increased. The final liquid on fractional crystallization at p_{O_2} = 0.21 atm. is the point *d* (fig. 5), whereas if p_{O_2} is increased to 1.0 atm., the final liquid is *b* (fig. 5).

Applying these considerations to figure 9, it is clear that if p_{O_2} increases during fractional crystallization a curve like *n-c-d* will apply to the composition of successive liquids, but the curve will lie below *n-c-d*. The greater the increase in p_{O_2} during crystallization, the farther below *n-c-d* will the curve lie. An example of a curve for the condition of increasing p_{O_2} is *n-b* of figure 9. This curve in figures 9a and 9b represents the change of liquid composition with perfect fractionation, starting with liquid *n* at p_{O_2} = 0.21 atm. and increasing the p_{O_2} at a regular rate until it reaches 1.0 atm. just as tridymite begins to separate. The liquid thus moves from the surface of figure 7 to that of figure 10, reaching the pyroxene-olivine-magnesioferrite univariant line at a point between *c* and *a* and the pyroxene-silica-magnesioferrite univariant line at *b*.

Families of curves of the type *n*-132-40-24, *n-c-d* and *n-b* of figure 9a and 9b thus exist representing change in the oxide ratio for perfectly fractionating liquids of initial compositions such as *n*. The attitude of a curve is determined by the direction and rate of change of p_{O_2}. Curves plotting FeO + Fe_2O_3/FeO

+ Fe_2O_3 + MgO against SiO_2, as in figure 9a, or FeO + Fe_2O_3/SiO_2 as in figure 9b are thus a means of estimating direction and amount of change in p_{O_2} during fractional crystallization.

In conclusion, for any selected composition in the tetrahedron of figure 5, families of crystallization curves can be constructed. For this discussion we have selected point *n*, a composition lying on the surface of p_{O_2} = 0.21 atm. This point resembles basalt. Similar curves will result starting with other points. The actual crystallization curves are very difficult to depict in the three dimensional space of the tetrahedron, although some types of curves have been shown with the aid of figure 6. Simplified curves however can be of much use, especially those obtained from a plot of FeO + Fe_2O_3/FeO + Fe_2O_3 + MgO against SiO_2 (fig. 9a). With perfect fractionation, the two extreme curves would be: (a) liquids moving with decreasing p_{O_2} to the fayalite-magnetite-silica eutectic in the right face of the tetrahedron, and (b) liquids moving with increasing p_{O_2} to the pyroxene-magnesioferrite-silica eutectic in the left face of the tetrahedron. In figure 9a, case (a) is illustrated by *n*-132-40-24. Case (b) is not shown. This latter would be a curve in figure 9a extending steeply downward to the right from *n*. The curve *n-b* is one where p_{O_2} increases five-fold during crystallization, while *n-c-d* is the case of constant p_{O_2}.

The curves of figure 9 are for fractional crystallization. In applying these considerations to problems of natural magmas it must be remembered that crystallization will be of a type intermediate between perfect equilibrium and perfect fractionation. The main effect of changing from perfect fractional crystallization to an intermediate type is to lower the slope and decrease the length of the curve *n*-132-40-24 in figures 9a and 9b, causing it to be more like *n-c-d* in direction and length. The curve *n-c-d* will not be changed by a decrease in degree of fractionation, except that the liquid will stop at *c* if perfect equilibrium is maintained.

CRYSTALLIZATION OF BASALTIC MAGMA

The analysis just given of crystallization paths in the system MgO–FeO–Fe_2O_3–SiO_2 has shown that fractional crystallization can produce two distinctly different trends in change of liquid composition. One trend will be taken if total composition of the mixture remains constant, and in this case p_{O_2} decreases during crystallization. The other trend is followed if p_{O_2} remains about constant or increases during crystallization, and in this second case the total composition changes by an increase in oxygen content for the compositions of special interest in this study. These trends are a natural and necessary consequence of the relations which exist among the phases: Mg-Fe olivines, Mg-Fe pyroxenes, and magnetite.[6] Despite the greater complexity of relations during crystallization of basaltic magma, the same type of trends may be expected during the early stages of crystallization when olivine, pyroxene and mag-

[6] In the preceding discussion the spinel phase has been called magnesioferrite, for it is most simply viewed as a solid solution of magnetite and magnesioferrite. The composition of this phase in equilibrium with liquid *c* (figs. 5, 7 and 8) is approximately 13MgO, 11FeO, 76Fe_2O_3. When referring to basaltic magma this spinel phase will be called magnetite, where titanium ions as well as magnesium occupy Fe^{2+} positions and other trivalent ions may substitute for part of the Fe^{3+}.

netite are principal phases, provided the two types of conditions are approached in nature: fractional crystallization at constant total composition of the mass, and fractional crystallization at constant or increasing p_{O_2}. Fractional crystallization undoubtedly occurs, but to a varying degree. The condition of constant total composition will be approached if the oxygen-containing gas phase is small compared to the mass of the condensed phases. The condition of constant or increasing p_{O_2} may be approached where sufficient water or carbon dioxide is present in the magma to give an appreciable p_{O_2} and to serve as a reservoir of oxygen to donate or accept oxygen from the liquid and crystalline phases without greatly changing its p_{O_2}. This will be discussed in a later section. Let us first see what trends we find in natural magmas, especially with respect to iron oxide, magnesia and silica. Do trends of change of liquid composition simulate those which occur in the system MgO–FeO–Fe_2O_3–SiO_2, and does it seem probable therefore that major lines of liquid descent can be explained as in this quaternary system by the manner of change of p_{O_2} during fractional crystallization?

Iron Oxide-Magnesia-Silica Trends in Basaltic Magma

Four series of chemical analyses have been plotted to ecompare trends of differentiating basaltic magmas with those established for mixtures in the MgO–FeO–Fe_2O_3–SiO_2 system. As representing tholeiitic basalts in general, Nockolds' (1954) averages have been used. Points I, II and III in figures 11a and 11b and table 2 are respectively: "tholeiitic olivine basalt", "normal tholeiitic basalt and dolerite," and "average tholeiitic andesite." Successive liquids of the Skaergaard intrusion according to Wager and Deer (1939), numbers Sk1, Sk2 and Sk3, are used as an example of a specific magma where differentiation by crystal fractionation is well established. Nockolds' (1954) three averages (points IV, V and VI) are used for the andesite-dacite-rhyodacite line of descent, while for a specific example of this type of magma series we have taken analyses of lavas from northwestern United States. The points labeled 2, 4, 5, 6 and 7 represent analyses of rocks selected by Turner and Verhoogen (1951) as representing the basalt-andesite association of the Cascade Province. The numbers for this last series correspond to those in Table XXI of these authors who list three olivine basalts. No. 2 was taken here as a representative olivine basalt from this province because it seems to be about average among those listed, not having the very large normative olivine content of their No. 1 nor the normative quartz of their No. 3. No. 4 is "basaltic andesite", No. 5 is "hpersthene andesite", No. 6 is "pyroxene andesite", and No. 7 is "porphyritic dacite." Analyses are listed in table 2.

If we compare figure 11a with figure 9a where the ratio of FeO + Fe_2O_3/FeO + Fe_2O_3 + MgO is plotted against SiO_2, and figure 11b with figure 9b where total iron oxide is plotted against SiO_2, a similarity of trends of curves is evident. The tholeiitic basalts and the Skaergaard liquids have trends like the liquids formed from fractional crystallization in the MgO–FeO–Fe_2O_3–SiO_2 system at constant total composition. The trends of the andesite-dacite-rhyodacite series and of the basalt-andesite-dacite association of the Cascades are like those of liquids crystallizing at constant p_{O_2}.

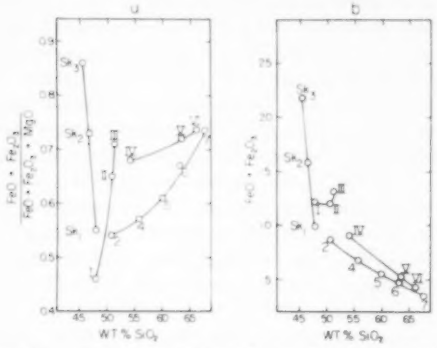

Fig. 11. Curves for magma series. Compositions of points are listed in table 2.

The curves for the Skaergaard liquids in figures 11a and 11b have a negative slope like the section 132-40-24 of the curves in figure 9, suggesting not only that fractional crystallization at constant total composition was the process by which successive liquids developed but also that the olivine-pyroxene surface was approximately reached by the "first liquid" of Wager and Deer (1939), No. Sk1. In analogy with mixture No. 132 of figure 9a, liquid Sk1 may have been derived from a tholeiitic olivine basalt from which considerable olivine had precipitated with movement of the liquid to the vicinity of the pyroxene-olivine surface.

Explanation of Table 2.

I—Tholeiitic olivine basalt, average after Nockolds (1954)

II—Normal Tholeiitic Basalt and dolerite, average after Nockolds (1954)

III—Tholeiitic andesite, average after Nockolds (1954)

IV—Andesite, average after Nockolds (1954)

V—Dacite plus dacite-obsidian, average after Nockolds (1954)

VI—Rhyodacite plus rhyodacite-obsidian, average after Nockolds (1954)

Sk1—First liquid of Skaergaard intrusion according to Wager and Deer (1939)

Sk2—Second liquid of Skaergaard intrusion according to Wager and Deer (1939)

Sk3—Third liquid of Skaergaard intrusion according to Wager and Deer (1939)

2—Olivine basalt (late Pleistocene); Lava Top Butte, Newberry volcano. Williams (1935). From Table XXI of Turner and Verhoogen (1951)

4—Basaltic andesite (Pleistocene) with 6.3 percent normative quartz; near summit of Crater Peak, southern Oregon, Williams (1942). From Table XXI of Turner and Verhoogen (1951)

5—Hypersthene andesite (Pleistocene) with 11.7 percent normative quartz; Crater Lake, southern Oregon. Williams (1942). From Table XXI of Turner and Verhoogen (1951)

6—Pyroxene andesite (Pleistocene) with 18.7 percent normative quartz; Mount St. Helens, Washington. Verhoogen (1937). From Table XXI of Turner and Verhoogen (1951)

7—Porphyritic dacite (sub-Recent) with 21.8 percent normative quartz; Medicine Lake highland, Anderson (1941). From Table XXI of Turner and Verhoogen (1951)

PC—Porphyritic Central type basalt, Mull. Bailey et al (1924). Representative analysis as given by Tilley (1950).

TABLE 2

Rock Analyses

	I	II	III	IV	V	VI	Sk1	Sk2	Sk3	2	4	5	6	7	PC
SiO_2	47.9	50.8	51.4	54.2	63.6	66.3	47.9	46.7	45.7	50.7	55.8	60.1	63.2	67.7	50
Al_2O_3	11.8	14.1	13.0	17.2	16.7	15.4	18.9	15.3	12.7	18.0	18.0	17.8	18.2	16.3	18
Fe_2O_3	2.3	2.9	3.4	3.5	2.2	2.1	1.2	2.9	3.6	1.6	2.6	2.0	1.4	0.3	9
FeO	9.8	9.0	9.7	5.5	3.0	2.2	8.7	12.9	18.2	7.0	4.1	3.4	3.3	3.2	
MgO	14.1	6.3	5.3	4.4	2.1	1.6	7.8	5.9	3.5	7.6	5.1	3.5	2.3	1.3	5
CaO	9.3	10.4	8.8	7.9	5.5	3.7	10.5	9.9	8.3	9.7	7.4	6.3	5.2	3.3	10
Na_2O	1.7	2.2	3.2	3.7	4.0	4.1	2.4	2.8	3.2	2.7	3.6	4.2	4.1	3.9	2.5
K_2O	0.5	0.8	1.0	1.1	1.4	3.0	0.2	0.3	0.4	0.7	1.2	1.3	1.2	3.2	0.4
TiO_2	1.6	2.0	2.6	1.3	0.6	0.7	1.3	2.2	2.4	1.3	0.8	0.5	0.5	0.3	1.0

The curves in figures 11a and 11b joining the analyses I, II and III resemble those for the section *n*-132-40 of curves in figure 9. The tholeiitic series of magmas like the Skaergaard liquids develop trends resembling those to be expected where crystallization is at constant total composition. For tholeiitic liquid series I-II-III, however, the initial liquid is sufficiently rich in MgO that olivine precipitates first without pyroxene, accounting for the initial positive slope of the curves. Note that in figure 11b the curve I-II-III has the strong concavity to the left as shown by *n*-132-40 of figure 9b.

In contrast to these, the liquids representing basaltic magma series of the orogenic belts have curves resembling *n-c-d*. The analogy is so striking that certainly it is reasonable to view point *c* (figs. 5, 7, 8 and 9) as andesite-like liquid and point *d* as dacite-rhyolite-like liquid, and to surmize that andesites and dacite-rhyolite lavas form from basalts by fractional crystallization under conditions approaching constant p_{O_2}. In further analogy with points *c* and *d*, andesites of the orogens are liquids from which Mg-Fe pyroxenes crystallize as olivine tends to react with the liquid and disappear, and dacites are the stage in liquid descent at which tridymite and pyroxene coprecipitate with a complete absence of olivine.

The curve 2-4-5-6-7 (fig. 11a) if extended to the left intersects I-II-III between I (tholeiitic olivine basalt) and II (normal tholeiitic basalt), whereas curve IV-V-VI extended to the left intersects I-II-III at a higher point. It is possible to conclude from this arrangement of curves that the immediate parent magma for each of these two series, 2-4-5-6-7 and IV-V-VI is a composition on the tholeiitic trend (I-II-III), with the primary magma for all basalts being an olivine basalt of a composition similar to point I. Accordingly a primary basalt liquid during crystal fractionation takes off from I and starts to follow a total constant composition trend characteristic of the magmas we call tholeiitic. If in its subsequent history a gas phase is introduced or develops which is capable of maintaining oxygen pressure more or less constant, or of causing it actually to increase, then the trend of change in liquid composition shifts to a subhorizontal direction. This latter direction of change in liquid composition is that leading to the normal andesites and dacites and rhyolites.

Subtraction Diagrams

The liquid lines of descent for factionally crystallized laboratory mixtures (fig. 9) are derived by assuming continuous separation of crystals from the liquid. At any stage during this fractionation a subtraction diagram can be constructed showing the amount and composition of the two fractions. If the crystallization has been at constant total composition, the lines on the diagram for all oxides will be straight, whereas if p_{O_2} has remained constant, the oxygen content of the mixture will usually have changed appreciably causing the lines for FeO and for Fe_2O_3 to have a significant discontinuity in their slopes. To illustrate this, subtraction diagrams have been constructed for the primary liquid *n* of figure 9 fractionally crystallizing under the two different oxygen pressure conditions to give liquids No. 132 and *c*. Following a discussion of

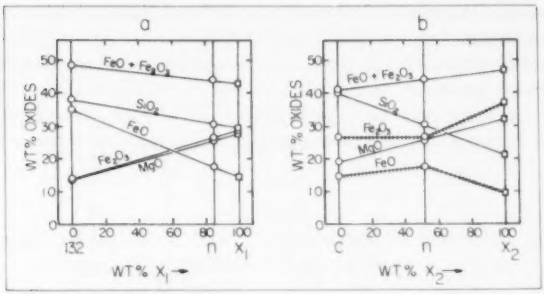

Fig. 12. Subtraction diagrams with mixture *n* of table 1 and figs. 8 and 9 as primary liquid. In (a) liquid 132 is derived by subtracting 85% as crystals of composition X_1. In (b) where constant p_{O_2} is maintained during fractional crystallization, liquid *c* is derived by subtracting 52% as crystals of composition X_2.

these cases, subtraction diagrams for basaltic magmas of figure 11 will be shown for comparison.

Mixture n in the system MgO–FeO–Fe_2O_3–SiO_2.—In figure 12a is shown the manner of derivation of liquid composition No. 132 (fig. 9 and table 1) from the primary liquid *n* by subtraction of the crystalline aggregate X_1. To construct this diagram it is necessary to make an estimate of the average composition of each crystalline phase. Then knowing the composition of liquids *n* and No. 132, the relative amounts of liquid and crystal fractions can be estimated. During fractional crystallization of *n* at constant total composition[7], the composition of the olivine changes from about $90M_2S$, $10F_2S$ to about $50M_2S$, $50F_2S$ at liquid No. 132. Taking into consideration the fact that early formed crystals will be in largest proportion in the crystalline aggregate, a reasonable estimate of the average composition of olivine during fractional crystallization of *n* as the liquid moves to point No. 132 is $75M_2S$, $25F_2S$. Pyroxene ranges in composition during this crystallization from about 88MS, 12FS to 55MS, 45FS, with an estimated average of 75MS, 25FS. The pyroxene coprecipitating with olivine at any temperature has a higher MS/FS ratio than the M_2S/F_2S ratio in olivine, but for mixture *n* much olivine has precipitated before pyroxene begins to crystallize with the result that the bulk composition of pyroxene has a ratio of FeO/MgO similar to that of olivine. The magnesioferrite precipitating has an average composition of about 55MF, 45FF. Using these compositions for the three crystalline phases separating while the liquid moves from *n* to No. 132, we find that approximately 85 percent of the mixture has separated as crystals. The chemical composition of the crystalline aggregate and the relative percentage of the phases is shown in table 3. It will be noted that the FeO and Fe_2O_3 lines, as well as others in figure 12a are straight as they must be under the assumption of constant total composition.

On fractionally crystallizing mixture *n* at constant p_{O_2}, the liquid moves

[7] Composition of olivine, pyroxene and magnesioferrite crystals appearing in the system MgO–FeO–Fe_2O_3–SiO_2 are given in terms of *weight percent* of the end members which are abbreviated as follows: M_2S = Mg_2SiO_4, F_2S = Fe_2SiO_4, MS = $MgSiO_3$, FS = $FeSiO_3$, MF = $MgFe_2O_4$, FF = $FeFe_2O_4$.

first to point *c* of figures 6, 7, 8 and 9. In figure 12b is a subtraction diagram showing the crystal fraction (X_2) separated from *n* to give *c*. Only olivine and magnesioferrite precipitate in this case, making calculations simple. Assuming that the olivine averages $88M_2S$, $12F_2S$ and the spinel 65MF, 35FF, 52 percent of the mixture has been precipitated as crystals during movement of liquid from *n* to *c* with the composition of the crystalline aggregate as shown in table 3.

TABLE 3

Composition of Crystalline Aggregates X_1 and X_2 subtracted from mixture *n* to give respectively liquids No. 132 and *c* (fig. 12)

	X_1	X_2
SiO_2	29.5	21.0
MgO	27.0	31.9
FeO	15.0	9.7
Fe_2O_3	28.5	37.4
Olivine	30.9* $75M_2S$, $25F_2S$	50.8 $88M_2S$, $12F_2S$
Magnesioferrite	38.2 55MF, 45FF	49.2 65MF, 35FF
Pyroxene	30.9* 75MS, 25FS	

* It just happens that in using the figure of 85% crystals, olivine and pyroxene are in equal proportions. With a smaller percent of crystals olivine is in larger amount, and with a greater percent of crystals pyroxene is in larger amount. With 87% of crystals, which is nearly as good a solution as 85%, 28.7% is olivine and 33.7% pyroxene. Formula designations are explained in footnote 7.

In figure 12b the striking feature is the discontinuity in the slope of the FeO and Fe_2O_3 lines. At the composition of the primary liquid, *n*, the FeO line has its maximum and the Fe_2O_3 line its minimum value. This change in direction of these two lines at the composition of *n* is a requirement where fractional crystallization is at constant p_{O_2}, except for the unusual case of no net gain or loss of oxygen during crystallization. Inasmuch as the iron content of crystals plus liquid must remain constant, the line representing total iron oxide is approximately straight. The chemical composition of the crystalline fraction and the proportion of this fraction which must separate from *n* to give *c* is thus readily obtained except that the ratio of Fe_2O_3 to FeO is known only after an assumption of composition of the crystalline phases. With the crystalline phases having the compositions as given above, the Fe_2O_3 and FeO content of the crystalline fraction follows directly. The Fe_2O_3 and FeO contents of liquids *n* and *c* are known from the diagram (fig. 7) and are given in table 1. In the process of fractionally crystallizing liquid *n* to produce liquid *c* and crystals X_2, 0.6 percent oxygen has been added to the mixture.

Basaltic magmas.—Turning to basalts, let us now consider subtraction diagrams that may result as basaltic magma differentiates by fractional crystllization. The close analogy of the curves I-II-III and 2-4-5-6-7 of figure 11a to *n*-132-40 and *n-c-d*, respectively of figure 9a has been noted. Subtraction diagrams deriving magma II from I and deriving magma 4 from 2 (fig. 11) should therefore be of the same nature as diagrams 12a and 12b, respectively,

for the curve I-II has the trend of *n*-132 where total composition remained constant, and the curve 2-4 the trend of *n-c* where p_{O_2} remained constant. Furthermore, the magmas numbered Sk1 and 2 in figure 11a lie close enough

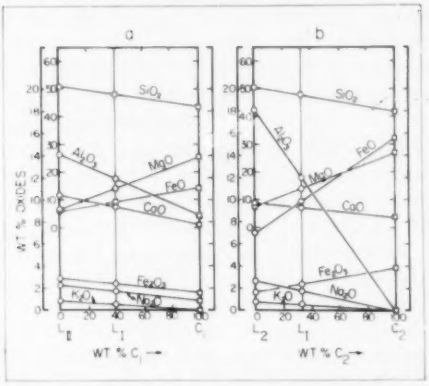

Fig. 13. Subtraction diagrams deriving by fractional crystallization liquids L_{II} and L_2 from primary tholeiitic olivine basalt, L_I. These liquids are respectively the composition II, 2 and I of table 2. The inside vertical scale applies to SiO_2 and MgO.

TABLE 4

Composition of Crystalline Aggregates C_1, C_2 and C_3*

	C_1	C_2	C_3
SiO_2	43.7	41.8	46.0
Al_2O_3	8.5	0.0	18.0
CaO	7.7	8.5	11.8
MgO	25.4	27.0	9.9
FeO	11.1	15.5	5.9
Fe_2O_3	1.5	3.8	4.4
Na_2O	0.85	0.0	2.2
K_2O	0.0	0.0	0.0
Plagioclase	27.2 Ab_1An_2	none	57.7 Ab_1An_2
Pyroxene	17.9 Di_4Fs_1	41.9 Di_4Fs_1	19.7 Di_3Fs_1
Olivine	51.7 Fo_4Fa_1	49.7 Fo_4Fa_1	14.4 Fo_3Fa_1
Magnetite	2.2	5.5	6.4

* C_1 and C_3 refer to crystalline aggregates subtracted from Tholeiitic Olivine Basalt, L_I to give respectively the Normal Tholeiitic Basalt liquid fraction (L_{II} of fig. 13) and the Orogenic Olivine Basalt fraction (L_3 of fig. 13). C_3 indicates crystalline aggregate subtracted from olivine basalt of Cascades to give Cascades basaltic andesite (fig. 14).

Summations are not 100 because TiO_2 and other minor constituents are omitted. Terms used in table 4 have the following compositions: Ab = $NaAlSi_3O_8$, An = $CaAl_2Si_2O_8$, Di = $CaMgSi_2O_6$, Fs = $FeSiO_3$, Fo = Mg_2SiO_4, Fa = Fe_2SiO_4, Magnetite = $FeO \cdot Fe_2O_3$. The mineralogical composition symbols are on a mol. percent basis.

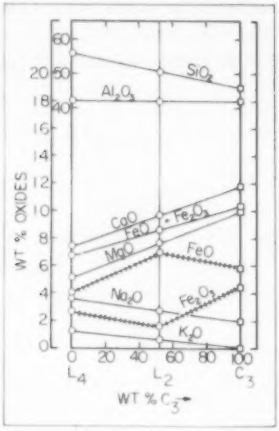

Fig. 14. Subtraction diagram deriving by fractional crystallization basaltic andesite, L_4, from olivine basalt L_2 (compositions 4 and 2 of fig. 11 and table 2), by subtracting 52% of crystalline aggregate C_3. The inside vertical scale applies only to SiO_2.

to the tholeiitic basalt line, I-II-III, that they also can be considered as derivatives of magma I by fractional crystallization at approximately constant total composition.

Subtraction diagrams are presented deriving magma II from I (fig. 13a), magma 2 from I (fig. 13b) and magma 4 from 2 (fig. 14). In each case the assumption has been made that the crystal fraction contains essentially no K_2O. Note that the FeO and Fe_2O_3 lines are straight in figures 13a and 13b, but contain a corner at the composition of the primary liquid in figure 14. The diagrams then have those features to be expected on the basis of comparing directions of curves in figure 11a with those of figure 9a; or in other words the sub-horizontal trend of curves in figure 11a develops as in figure 9a as a consequence of fractional crystallization at approximately constant p_{O_2} and the vertical trend as a consequence of fractional crystallization at approximately constant total composition. Details regarding these subtraction curves and their implications are developed in the two sections following.

(a) *Tholeiitic and high alumina basalts.* Normal tholeiitic basalts contain about 13 to 15 percent Al_2O_3 and occur chiefly in non-orogenic regions. Basalts and andesites of orogenic belts on the other hand are characteristically of a high-alumina variety, as recently emphasized by Tilley (1950). These latter contain of the order of 17 to 19 percent Al_2O_3, and although typical of the orogens are found in a few other interesting spots. It will be noted from table 2 that the olivine basalt, 2, and basaltic andesite, 4, of the Cascade orogenic belt are of the typical high-alumina variety, and that also the Skaergaard first liquid, Sk1, and Porphyritic Central type, PC, are high-alumina basalts. Subtraction diagrams deriving the normal tholeiitic basalt, II, and the high alumina basalt, 2, from the same primary tholeiitic olivine basalt, I

(fig. 13), provide an interesting comparison, as well as a clue to the origin of the high-alumina basalts.

The diagrams of figures 13a and 13b develop readily on decreasing the K_2O content to zero at the vertical line repreesnting composition of the crystalline fraction. This fixes the percent of the crystalline and the derived liquid fractions and the chemical composition of the former. Thus in figure 13a, with 40 percent of crystalline fraction of composition C_1 subtracted from L_I, the normal tholeiitic basalt liquid II develops. The mineralogical composition of C_1 is estimated to be as shown in table 4.

In deriving liquid L_2 (olivine basalt 2) from L_I by separation of a crystalline fraction (fig. 13b), it is found, perhaps surprisingly, that Al_2O_3 and Na_2O decrease to zero in the crystalline fraction essentially simultaneously with K_2O. This occurs with 33 percent C_2, 67 percent L_2. The crystalline aggregate of composition C_2 can contain no feldspar. This suggests that the high-alumina basalts develop from tholeiitic olivine basalt by fractional crystallization under conditions such that plagioclase is delayed in separating.

The subtraction diagrams of figure 13 are significant in illustrating: (a) that a common parent is probable for the normal tholeiitic and the high alumina basalts, (b) that the high alumina content of the latter results from a lack of separation of plagioclase from the liquid at this differentiation stage, and (c) that the normal tholeiitic basalts and this particular high-alumina olivine basalt of the Cascade region were very likely derived by fractional crystallization under conditions of approximately constant total composition.

In the environments in which the high-alumina basalts typically develop apparently plagioclase crystals do not readily settle out of the basalt liquid. Possibly turbulence or convection currents characterize basalt and andesite liquids crystallizing in orogenic belts, and this movement within the liquid is a factor in keeping plagioclase crystals in suspension. A statement by Waters (1955) is of interest in this connection. In discussing the pyroxene andesites and basaltic andesites of the Cascade orogenic belt, he says, "Despite the great range in silica content, the rocks have certain features in common. They are characterized by high lime and alumina and are relatively low in iron. Most are crowded with phenocrysts of plagioclase that show a complex combination of oscillatory and progressive zoning." These observations are compatible with the idea that plagioclase crystallized but tended to remain in suspension. There is another possibility. Some of the high alumina magmas originating in orogenic belts may have had plagioclase crystallization supressed until a lower temperature point because of high water pressure. The experiments of Yoder (1954) indicate that the diopside-anorthite eutectic is shifted toward anorthite with increasing water pressure. Water pressure might therefore be a factor in causing delay in the appearance of plagioclase as a crystalline phase in certain of the high-alumina magmas.

Two other high alumina basalts, both of the Brito-Arctic region, are listed in table 2, labeled Sk1 and PC. Their compositions are very similar to that of the Cascade olivine basalt (no. 2, table 2), and hence can be derived from tholeiitic olivine basalt just as L_2 was derived from L_1, in figure 13. One is tempted to view both the "first liquid" of the Skaergaard and the Porphyr-

itic Central type of Mull as magmas derived from a tholeiitic olivine basalt from which plagioclase was reluctant to separate. From petrologic evidence this would seem to be a not unreasonable conclusion with regard to the Porphyritic Central type. Wager and Deer (1939), however, believe that Sk1 is the primary liquid for the Skaergaard rocks and that is was "free from porphyritic plagioclase crystals when intruded".

(b) *Basalts and andesites of orogenic belts.* The series of Cascade magmas, 2-4-5-6-7 (table 2), is taken as representative of basalt-andesite suites of orogenic belts. As discussed earlier, the subhorizontal trend of the iron oxide-magnesia ratio line (fig. 11a) points to the formation of this series by fractional crystallization under conditions of approximately constant p_{O_2}. The subtraction diagram (fig. 14) where all of the major oxides are considered bears out this conclusion. In this diagram basaltic andesite, 4, of table 2 (L_4 of fig. 14) is derived from olivine basalt 2 (L_2) by subtraction of the crystalline fraction, C_3. The FeO and Fe_2O_3 lines in figure 14 have maxima and minima respectively at the vertical line representing the composition of the primary magma. Oxygen has been added to the total mass during fractionation, just as in the case of derivation of liquid, *c*, and crystalline fraction, X_2, of figure 12b. The fractions, L_4 and C_3 have a combined oxygen content 0.2 percent greater than the oxygen content of original magma, L_2.

The subtraction diagram of figure 14 is constructed by first finding the position for the vertical line representing the original magma, L_2, such that the K_2O line decreases to zero at composition of the crystalline aggregate, C_3. This occurs where the proportions of C_3 and L_4 are 52 and 48 percent respectively, by coincidence the same percentages found in deriving liquid *c* and X_2 from *n* (fig. 12b). Magnetite is assumed to have its stoichiometric composition, and plagioclase, pyroxene and olivine have compositions as given in table 4. Here the olivine has been assigned the mole composition, 90 Mg_2SiO_4, 10 Fe_2SiO_4, and plagioclase has the composition Ab_1An_2. Pyroxene then has the composition 40 $CaSiO_3$, 40 $MgSiO_3$, 20 $FeSiO_3$; and there is 6.4 percent magnetite. If olivine is assumed to have the composition 80 Mg_2SiO_4, 20 Fe_2SiO_4, as it was in C_1 and C_2, the pyroxene composition will have the higher Di:Fs ratio of 3:1, and the percent of magnetite will be reduced to 5.4. The mineralogical composition of C_2 (table 4) is thus by way of example. A reasonable olivine composition is assumed, and then this determines the MgO:FeO ratio in the pyroxene, the amount of magnetite, and the amount of O_2 which must be added to convert part of the FeO in L_2 to Fe_2O_3 in L_4 and C_3.

Conclusions Regarding Tholeiitic Basalt Derivative Magmas

From these considerations, and referring again to figure 11, we arrive at these following general conclusions. Tholeiitic basalt magmas of the orogens and of the non-orogens both have as a common parent a basalt of the general nature of Nockolds' average tholeiitic olivine basalt. With fractional crystallization one of two main trends will be followed. Where total composition remains about constant during crystallization, with a consequent decrease in p_{O_2}, a trend of the type exhibited by I-II-III and Sk1-Sk2-Sk3 curves in figure 11a

is followed. This trend we note in the vast outpouring of lavas in the non-orogenic regions and in magmas of sheet intrusions, and apparently also in achondritic meteorites (Buddington, 1943). Where p_{O_2} has remained about constant or increased during fractional crystallization, curves for successive liquids follow trends such as 2-4-5-6-7 and IV-V-VI (fig. 11a). These trends are characteristic of the basalt-andesite series of orogenic belts.

These principal trends are a function of the manner of change of p_{O_2} during fractional crystallization. A secondary effect relating to the degree of separation of plagioclase from the liquid during the early stages of crystallization may be superimposed upon the main trends. If plagioclase fails to separate from the liquid in the proportions to be expected from fractional crystallization, high-alumina magmas form, characteristic of basalts and andesites of orogenic belts, but also found among some other magmas. This alumina effect is not noticed on the diagram of figure 11a because only MgO, iron oxide and SiO_2 are considered there, but is clearly evident in the subtraction diagrams (fig. 13).

CONSTANCY OF p_{O_2} RELATED TO WATER PRESSURE

The conclusion seems inescapable that manner of change of oxygen pressure during fractional crystallization of basaltic magmas is the chief control determining whether the liquids move toward higher silica and lower iron oxide content (calc-alkali trend) or toward higher iron oxide with little change in silica content (tholeiitic trend). The former occurs where p_{O_2} remains about constant or increases, and this entails addition of oxygen to the system. Inasmuch as this is the trend of basaltic magmas differentiating in orogenic belts, a mechanism presumably exists in these environments for maintaining a nearly uniform or increasing level of p_{O_2} during crystallization. A higher water content in these magmas during differentiation is probably the principal factor.

Water dissociates according to the equation $2H_2O = 2H_2 + O_2$. With increasing temperature and pressure, p_{O_2} increases. From Kennedy's (1948) table we learn that at 1200° and 100 atm. of water pressure, p_{O_2} has attained the value of 1.5×10^{-3} atm. At this same temperature and 3000 atm. water pressure the figure is 1.5×10^{-2} atm. It is the oxygen from this reaction that may account for maintenance of an approximately constant p_{O_2} during crystallization.

The p_{O_2} from dissociation of water will increase or decrease or remain about constant during crystallization depending upon the balance which may be established among several factors. Two operate to decrease p_{O_2}: (1) Falling temperature causes a decrease in dissociation of water for a given water pressure. (2) If the basalt or andesite magma is to crystallize at constant p_{O_2} it must continually take a small amount of oxygen from the water, and this tends to decrease the oxygen and increase the hydrogen partial pressure. These two effects however may be counterbalanced and perhaps actually over compensated for by two other factors: (1) As crystallization of anydrous minerals proceeds, the amount of liquid phase in which water is dissolved decreases. The percent of water in the magma therefore increases with a concomitant increase in water pressure and hence p_{O_2}. (2) At these temperatures the rate of

diffusion of hydrogen through the silicate liquid and into the country rock toward regions of lower hydrogen partial pressure must be appreciable. Hydrogen pressure therefore probably does not build up significantly as oxygen from dissociation of water enters the crystalline and liquid silicate structures. Loss of hydrogen by diffusion would affect the equilibrium in the direction of increasing p_{O_2}.

Specific experimental data are needed to make quantitative estimates on the manner of change of p_{O_2} during crystallization of basaltic magma at various water pressures, but from these general considerations we see that it should not be unexpected that the p_{O_2} will remain about constant or increase as a magma crystallizes if water pressure is appreciable. Inasmuch as the other lines of evidence as discussed in the previous sections lead to the conclusion that p_{O_2} did remain about constant during crystallization of magmas of orogenic belts, we conclude that this is a natural effect of an appreciable water content. Supplementing the p_{O_2} from dissociation of water is that from dissociation of CO_2 and other oxygen-containing gases, but in the usual case water certainly must be the principle source of oxygen.

We may speculate that a basaltic magma entering a geosynclinal belt will absorb water (and CO_2) from the sediments as these rocks are squeezed, heated and their minerals dehydrated (and decarbonated) through formation of higher temperature suites. We have little information on the solubility of water or of CO_2 in a silicate liquid of basalt composition as a function of temperature and pressure, but we know that at only one atmosphere of steam pressure water enters simple silicate glasses very readily (Kurkjian, 1958). As the water pressure increases solubility of water will increase, finally leveling off at very high pressures. Water from the sediments of a geosyncline should therefore be absorbed easily by basaltic magma as it moves into these sediments and raises their temperature. The explosive nature of lavas of orogenic belts is suggestive of a high water pressure, and the wide spread serpentinization and other aspects of hydrothermal activity in these belts again attest to the presence of abundant water associated with the magmas of the orogens.

CONCLUSION

The manner of change of p_{O_2} during fractional crystallization of an iron oxide-containing silicate liquid can have a profound effect on the course of crystallization. That this bears importantly on the crystallization and differentiation of basaltic magmas seems evident from the preceding discussion. Basalts have a sufficiently high iron oxide content that the matter of whether p_{O_2} decreases or not is of great significance in determining the course of the liquid. The p_{O_2} of a basalt decreases if total composition remains constant during crystallization, and this happens if oxygen is not available from a gas phase for addition to the condensed phases. If oxygen is available, p_{O_2} decreases at a slower rate, remains about constant, or increases. The successive liquids of the Skaergaard differentiated intrusion typify crystallization at constant total composition. The olivine basalt-basaltic andesite-andesite-dacite series of lavas of the Cascade orogenic belt is taken as an example of liquids developing by

fractional crystallization under conditions such that the p_{O_2} decreased at a much slower rate and perhaps actually increased during crystallization. Water in the latter series of liquids is believed to have been present in sufficient amounts that with slow cooling and crystallization in a magma reservoir the p_{O_2} was maintained at something of the order of of a constant value, supplying an estimated 0.2 percent oxygen to the condensed phases during change of liquid from olivine basalt to basaltic andesite.

We may speculate that the normal calc-alkali series of igneous rocks develops by fractional crystallization of tholeiitic olivine basalt magma which intrudes orogenic belts and differentiates in the manner proposed for the Cascade liquids; whereas this same primary magma entering non-orogenic regions differentiates along the path demonstrated for the Skaergaard. The first leads toward increasing silica with continuous decrease in iron oxide. The second leads to increase in iron oxide, accompanied by little change or actual decrease in silica until the very last stages of crystallization. The first develops liquids which solidify to such common rocks as andesite, dacite, rhyolite, granodiorite and granite; the second tends to develop the uncommon ferrogabbros with a small amount of a final felsic residue. The accumulative crystalline fraction complement of the calc-alkali liquid fraction is presumably represented by the common peridotites and serpentinites and other ultramafic rocks of the orogenic belts.

If the above is true, why do primary basaltic magmas intruding in orogenic belts take this course of differentiation leading to such different products from those intruding in non-orogenic regions? A partial answer would seem to be that it is in the orogenic belts that the primary basalt can and usually does pick up water. The amount of water required to prevent the p_{O_2} from significantly decreasing during the early stages of crystallization and hence to cause the differentiating liquid to move toward the andesite-dacite-rhyolite series cannot be calculated at present. Probably only a very few percent would be required at the start of crystallization. With the usual minerals crystallizing, the p_{H_2O} will increase rapidly to maintain a roughly constant or possibly even an increasing p_{O_2} despite the absorption of a few tenths of one percent of oxygen by the condensed phases.

Although water content can, we believe, explain the difference in trend of differentiation, there are at least two other major questions of interest here: (a) Why does extensive differentiation of this primary basalt usually take place when emplaced in orogenic belts, whereas in the non-orogenic regions the primary basalt is usually not greatly differentiated, and (b) Why are igneous rocks of the orogenic belts largely intrusive and granitic and those of the non-orogenic regions largely extrusive and basaltic? These questions are closely related. Part of the answer apparently lies in the fact that primary basalt intruding orogenic belts commonly can accumulate in a large pool or reservoir for slow cooling and differentiation, whereas similar magma entering other regions does not usually have the opportunity of expanding into a reservoir. Whether the former is able to make its own reservoir because it moves from a higher pressure region into relatively incompetent geosynclinal sediments that can be pushed aside and upward is a matter of conjecture, but

that huge batholithic reservoirs existed seems apparent from geologic relations. Slow cooling in these reservoirs would inevitably cause extensive differentiation by fractional crystallization, and resulting rocks would be coarse-grained and intrusive except as some of the liquid escaped to the surface from time to time as basalt, andesite, dacite, rhyolite and related extrusives.

In contrast, the same primary basalt moving upward through the crust in non-orogenic regions typically moves directly to the surface through fissures in the competent crust with only occasionally a sheet-like reservoir and hence with only an occasional chance for a high degree of differentiation. A case in point is the Cascade province of Washington about which Waters (1955) states: "A striking feature of Cascade geology is the predominant andesitic activity along the Cascade axis at the same time vast amounts of tholeiitic basalt were being erupted on either side." This andesitic lava logically represents liquid escaping from a large reservoir of originally basaltic magma in the orogenic belt, differentiating by fractional crystallization under conditions approaching constant p_{O_2}, whereas the basaltic magma entering the crust outside of the geosyncline has not had an opportunity to differentiate. That the intrusive rocks of the world are largely granodiorite and granite whereas the extrusives are predominantly basalt may be tantamount to saying that basaltic magma entering orogenic belts has an opportunity usually of cooling slowly at depth and of picking up water resulting in differentiation by fractional crystallization to give granodiorite and granite, whereas basaltic magma of non-orogenic regions usually comes to the surface with little chance for slow cooling and differentiation and hence solidifies as extrusive basalt.

The concept that basaltic magma entering orogenic belts normally has an opportunity to cool slowly and differentiate extensively in the direction to produce the calc-alkali series of rocks explains the relatively small volume of gabbro in orogenic belts as compared with the large volume of products of differentiation such as granodiorite, but also requires that the complementary ultramafic rocks be present in large volume in these belts, although in general at greater depth than the granitic rocks. Accumulative ulramafic rocks formed as complements to the granodiorites and granites are presumably represented by the extensive serpentinites, peridotites and dunites of the orogenic belts. In the main, these have apparently been forced upward to present positions as largely crystalline intrusions. Hess (1955) does not look upon these ultramafic rocks as being accumulative types, but his arguments seem to be based at least partly on the assumption that ultramafic crystal accumulates can only be of the type found in strataform sheets—that is, where fractional crystallization is of the constant total composition variety. If the possibility of fractional crystallization of basaltic magma under conditions approaching constant p_{O_2} is granted, and this we infer to be characteristic of orogenic belts, then a different conclusion is possible. Just as the liquids follow a different trend depending on the p_{O_2} conditions under which fractional crystallization occurs, so will their complementary crystalline fractions.

ACKNOWLEDGMENTS

I wish to thank members of the staff of the Department of Mineralogy and Petrology, Cambridge, England, for their many courtesies, and particularly C. E. Tilley, S. R. Nockolds and S. O. Agrell for stimulating discussions on igneous rock problems. Work on this paper was pursued at Cambridge during the spring of 1958. I am also indebted to my colleague Arnulf Muan with whom many discussions have taken place on problems of iron oxide systems. The tour of study in England was facilitated by a National Science Foundation Senior Post-Doctoral Fellowship.

REFERENCES

Andersen, Olaf, 1915, The system anorthite-forsterite-silica: Am. Jour. Sci., v. 39, p. 407-454.

Anderson, C. A., 1941, Volcanoes of the Medicine Lake highland, California: Calif. Univ., Dept. Geol. Sci. Bull. v. 25, p. 347-422.

Bailey, E. B., Thomas, H. H., and others, 1924, The Tertiary and post-Tertiary geology of Mull, Lock Aline and Oban: Scotland Geol. Survey Mem.

Bowen, N. L., 1947, Magmas: Geol. Soc. America Bull., v. 58, p. 263-280.

Bowen, N. L., and Schairer, J. F., 1935, The system MgO–FeO–SiO_2: Am. Jour. Sci., v. 29, p. 151-217.

Buddington, A. F., 1943, Some petrologic concepts and the interior of the earth: Am. Mineralogist, v. 28, p. 119-140.

Fenner, C. N., 1929, The crystallization of basalts: Am. Jour. Sci., v. 18, p. 225-253.

————, 1948, Immiscibility of igneous magmas: Am. Jour. Sci., v. 246, p. 465-502.

Hess, H. H., 1955, Serpentines, orogeny, and epeirogeny: Geol. Soc. America, Sp. Paper 62, Crust of the Earth, p. 391-408.

Kennedy, G. C., 1948, Equilibrium between volatiles and iron oxides in igneous rocks: Am. Jour. Sci., v. 246, p. 529-549.

————, 1955, Some aspects of the role of water in rock melts: Geol. Soc. America, Sp. Paper 62, Crust of the Earth, p. 489-503.

Kurkjian, C. R., 1958, Solubility of water in molten alkali silicates: Soc. Glass Tech Jour., v. 42, p. 130-144.

Muan, A., 1955, Phase equilibria in the system FeO–Fe_2O_3–SiO_2: AIME Trans., v. 203, p. 965-967, Jour. Metals, Sept. 1955.

————, 1958, Phase equilibria at high temperatures in oxide systems involving changes in oxidation states: Am. Jour. Sci., v. 256, p. 171-207.

————, and Osborn, E. F., 1956, Phase equilibria at liquidus temperatures in the system MgO–FeO–Fe_2O_3–SiO_2: Am. Ceram. Soc. Jour., v. 39, p. 121-140.

Nockolds, S. R., 1954, Average chemical compositions of some igneous rocks: Geol. Soc. America Bull., v. 65, p. 1007-1032.

Tilley, C. E., 1950, Some aspects of magmatic evolution: Geol. Soc. London Quart. Jour., v. 106, p. 37-61.

Turner, F. J., and Verhoogen, J., 1951, Igneous and metamorphic petrology: New York, McGraw-Hill Book Co.

Verhoogen, J., 1937, Mount St. Helens, a recent Cascade volcano: Calif. Univ., Dept. Geol. Sci., Bull., v. 24, p. 293.

Wager, L. R., and Deer, W. A., 1939, Geological investigations in East Greenland, part III. The petrology of the Skaergaard intrusion, Kangerdlugssuaq, East Greenland: Medd. om Grønland, v. 105, no. 4, p. 1-335.

Waters, A. C., 1955, Volcanic rocks and the tectonic cycle: Geol. Soc. America, Sp. Paper 62, Crust of the Earth, p. 703-722.

Williams, H., 1935, Newberry volcano of central Oregon: Geol. Soc. America Bull., v. 48, p. 295.

————, 1942, The geology of Crater Lake National Park, Oregon: Carnegie Inst. Washington, Pub. 540, p. 149.

Yoder, H. S., Jr., 1954, The system diopside-anorthite-water: Annual report of the director of the Geophysical Laboratory, Carnegie Inst. Wash. Year Book, No. 53, p. 106-107.

[American Journal of Science, Vol. 257, November 1959, P. 648-655]

EFFECT OF CARBON DIOXIDE ON THE MELTING OF GRANITE AND FELDSPARS*

P. J. WYLLIE and O. F. TUTTLE

Department of Geophysics and Geochemistry, College of Mineral Industries, Pennsylvania State University, University Park, Pennsylvania

ABSTRACT. Unlike water vapor and fluorine, carbon dioxide under pressure has little or no effect on the rates of melting or crystallization of granite or alkali feldspars, and the melting temperatures are apparently unaffected except insofar as pressure per se raises the temperature of melting. The melting temperature of granite in the presence of a mixture of carbon dioxide and water vapor at a fixed total pressure is raised if the proportion of carbon dioxide in the vapor is increased, indicating that carbon dioxide is less soluble in granitic liquids than is water. Although the solubility of carbon dioxide in granitic liquids is too small to be determined directly by the techniques used, any appreciable solubility would produce a measurable lowering of the melting temperature. It is suggested that the solution of carbon dioxide in silicate liquids depends upon the availability of cations which are not structurally bound to the silicate network of the liquid and are therefore available for carbonate formation in the liquid.

INTRODUCTION

The role of volatile materials in igneous and metamorphic processes has long been a subject for speculation among geologists. Experimental data are now available on the effect of water vapor under pressure on many silicate systems, but little is known of the effect of other volatiles. The authors are engaged in a study of ternary systems containing water and a second volatile component, and quantitative data have been obtained for several systems by enclosing measured proportions of silicate and two volatile components in small thin-walled sealed platinum or gold capsules and applying pressure by collapsing the tubes with water vapor under pressure. Preliminary results have been presented (Wyllie and Tuttle, 1957; Tuttle and Wyllie, 1957). Our early efforts were directed toward systems containing water and carbon dioxide, but experimental difficulties prohibited use of the sealed capsule method with these volatiles. However, qualitative results were obtained in an open system and because carbon dioxide, after water, is probably the most abundant volatile material in the earth's crust, we are presenting these results here.

It was expected that the fluxing action of carbon dioxide would be almost as effective as that of water, but instead it was found that dry carbon dioxide is relatively insoluble in feldspathic and granitic liquids; equilibrium was not attained in runs lasting two or three days, and dry carbon dioxide under pressure appeared to produce little change in melting temperatures of the silicates studied. When the vapor phase around the sample consisted of a mixture of water vapor and carbon dioxide, the melting temperatures of the silicates were raised as the proportion of carbon dioxide was increased at constant pressure.

STARTING MATERIALS AND EQUIPMENT

Silicates used as starting materials were: (1) Westerly granite (Rhode Island) and the homogeneous glass produced by repeated fusion and crushing of the granite, (2) synthetic albite glass and albite crystallized hydrothermally

* M. I. Experiment Station Contribution No. 58-66.

from the glass, and (3) synthetic $Ab_{70}Or_{30}$ glass and crystals grown hydrothermally from the glass. The volatile components used were bone dry carbon dioxide from Matheson and Company, and ion-exchange water.

Experiments were carried out in cold-seal pressure vessels (Tuttle, 1949). The complete apparatus and the method used for pumping carbon dioxide under pressure into the system have been described in detail by Harker and Tuttle (1955).

RESULTS

Effect of Water.—PT curves for the beginning of melting of Westerly granite and for complete melting of the synthetic feldspars in the presence of excess water vapor are known (Tuttle and Bowen, 1958). The lowering of melting temperatures produced by water vapor is considerable in each example and equilibrium is attained in runs lasting a few hours.

Effect of Carbon Dioxide.—The silicate charges, contained in small gold or platinum crucibles within the pressure vessel, were held at constant temperature and pressure in an atmosphere of carbon dioxide. The pressure vessel was quenched in cold water at the end of the run and the crushed charges were examined using a petrographic microscope. Forty-three charges were held between the "dry" melting temperatures of the silicates and the PT curves for the beginning of melting of the silicates in the presence of water vapor under pressure. The duration of the runs ranged from 3 to 63 hours. No melting was observed in crystalline charges and a few very small crystals grew in charges of glass. The quantity of crystals was not sufficient to yield x-ray powder diffraction patterns. It is evident that equilibrium was not attained, but the growth of crystals in the glasses indicates the direction of equilibrium. It is probable that the melting temperatures of granite and alkali feldspar are lowered little, if at all, by carbon dioxide under pressure, but the high PT conditions and the slow rate of reaction prohibited the determination of melting curves.

These runs demonstrate that the action of dry carbon dioxide under pressure is very different from that of water. The size and nature of the crystals which grew in the charges of glass are comparable with those which grow under dry conditions at atmospheric pressure, whereas in the presence of water vapor under pressure feldspar glasses crystallize completely within a few minutes.

Effect of Water and Carbon Dioxide.—Various methods were considered for sealing a ternary mixture of silicate, water, and carbon dioxide in known proportions into a small capsule. In order to obtain useful results it is necessary to seal repeatedly the same proportions of silicate and the two volatiles within a capsule. None of the methods tried was satisfactory and we turned to an open-system technique. The silicate charges were held in small gold crucibles within the pressure vessel and the pressure was applied by a mixture of water and carbon dioxide.

It is difficult to obtain a homogeneous mixture of two volatile components under pressure. If the required total pressure is obtained in two stages by pumping water into the system first, followed by carbon dioxide, the gases do

not mix freely and the results are similar to those obtained with the same total pressure of water vapor. Similarly, if carbon dioxide is pumped into the system first, followed by water, the charges behave as if the total pressure were applied by carbon dioxide. Harker (1958) carried out extensive experiments in the system $MgO—CO_2—A$ and he found that the only satisfactory method of obtaining a homogeneous atmosphere within a pressure vessel is to mix the gases in the pump prior to their compression and injection. Unfortunately water and carbon dioxide do not mix as freely as argon and carbon dioxide, and it would be difficult (perhaps impossible) to obtain a homogeneous phase consisting of water and carbon dioxide in the pump at room temperature.

It was found that when a trace of water was present in the system, and when the required total pressure was applied by carbon dioxide, the rate of reaction was quite rapid, and the results were different from those obtained in the presence of water vapor or carbon dioxide alone. Several methods of adding measured amounts of water to the system and of applying pressure with carbon dioxide were attempted and, provided a standard procedure was followed, consistent results were obtained with each method. The standard procedure adopted was as follows: The charges were supported within a small cup at the top of a rod which almost filled the space within the pressure vessel, and measured amounts of water were pipetted into the cup. The pressure

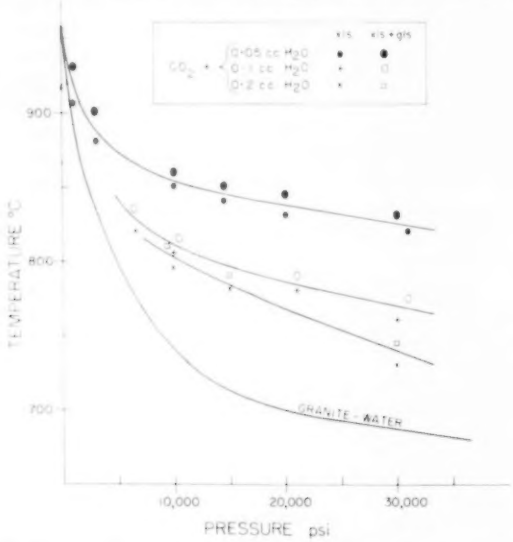

Fig. 1. The "system" granite—water—carbon dioxide. PT curves comparing the depression of beginning of melting of Westerly granite in the presence of water vapor with the effect of various mixtures of water vapor and carbon dioxide. When the amount of water vapor is decreased (i.e., the partial pressure of carbon dioxide is increased) at constant pressure, the temperature of beginning of melting is raised. psi = pounds per square inch; xls = crystals; gls = glass.

vessel was connected to a reservoir of carbon dioxide at a pressure of 900 psi and the temperature was raised rapidly to the required level. The low initial pressure of carbon dioxide served to keep the water near the sample when it vaporized. Carbon dioxide was pumped into the system when the temperature reached the desired value.

PT curves for the beginning of melting of the granite were determined in this way using different amounts of water (0.05 cc, 0.1 cc, and 0.2 cc). The runs which fixed the PT curves are listed in table 1 and are plotted in figure 1 where they are compared with the curve obtained in the presence of water vapor alone. With 0.05 cc water in the system the temperature of beginning of melting of granite is lowered by 85°C at 5000 psi total pressure. Increasing the total pressure to 30,000 psi depresses the melting temperature by a further 50°C. The PT curves obtained using 0.1 cc and 0.2 cc water are successively lower; the PT curve with 0.2 cc water in the system is about 50°C higher than

TABLE 1

Results of Melting Experiments in the "System" Granite—Water—Carbon Dioxide

Abbreviations: psi = pounds per square inch; xls = crystals; gls = glass

Pressure psi	Temp. °C	Time Hrs.	Result
	0.05 cc water, plus carbon dioxide pressure		
1,000	905	25	xls
1,000	930	65	xls + gls
3,000	880	22	xls
3,000	900	23	xls + gls
10,000	850	26	xls
10,000	860	24	xls + gls
14,500	840	24	xls
14,500	850	21	xls + gls
20,000	830	23	xls
20,000	845	17	xls + gls
31,000	820	2	xls
30,000	830	2	xls + gls
	0.1 cc water, plus carbon dioxide pressure		
6,500	820	24	xls
6,500	835	18	xls + gls
10,000	805	18	xls
10,500	815	21	xls + gls
21,000	780	23	xls
21,000	790	19	xls + gls
30,000	760	2	xls
31,000	775	2	xls + gls
	0.2 cc water plus carbon dioxide pressure		
10,000	795	23	xls
9,500	810	24	xls + gls
15,000	780	24	xls
15,000	790	22	xls + gls
30,000	730	25	xls
30,000	745	3	xls + gls

that obtained in the presence of water vapor alone. At a total pressure of 30,000 psi the temperatures of beginning of melting in the presence of 0.05 cc, 0.1 cc, and of 0.2 cc water (plus carbon dioxide) are 825°C, 770°C, and 740°C, respectively. In the presence of water vapor alone at this pressure, the melting temperature is 685°C. The effect of increasing the volume of water added to the system is to increase the ratio of water vapor to carbon dioxide in the atmosphere around the sample. Therefore the temperature of beginning of melting at any pressure is raised as the proportion of carbon dioxide in the vapor phase is increased (fig. 1).

If 0.1 cc water is placed within the pressure vessel and the temperature is raised to about 800°C, the pressure in the system is less than 50 psi. However, during a run the partial pressure of water vapor in the mixed atmosphere around the samples would certainly be greater than this because the experimental method employed tends to hold the water vapor near the sample, although there is probably some diffusion of water away from the sample in response to the temperature gradient within the vessel. The results show that the carbon dioxide does not act solely as a piston, holding the water vapor in an envelope around the sample; if this were the case, the results obtained with different amounts of water would be identical with the results obtained in the presence of water vapor alone. There must be some mixing between the carbon dioxide and water. Although the proportions of water vapor and carbon dioxide around the samples were not known, the fact that different PT curves were obtained using different amounts of water demonstrates that the partial pressure of water vapor in the atmosphere around the sample differed from one set of conditions to another. The ratio of carbon dioxide to water vapor around the sample probably varies to some extent along each PT curve in response to changing pressure, but the range of this variation must be slight compared to the differences existing between the ratios for different PT curves.

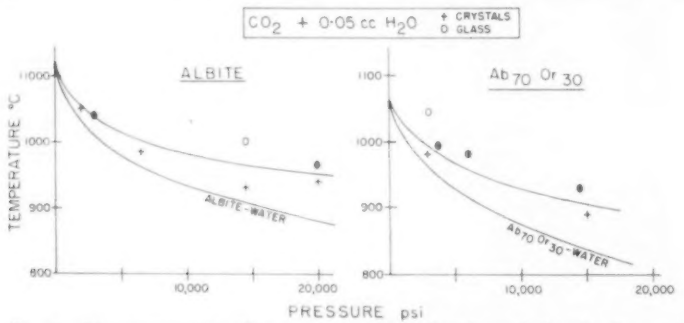

Fig. 2. The systems (a) albite—water—carbon dioxide, and (b) $Ab_{70}Or_{30}$—water—carbon dioxide. Preliminary PT curves comparing the depression of melting temperature of synthetic feldspars in the presence of a mixture of water vapor and carbon dioxide with the effect of water vapor alone. The addition of carbon dioxide to water vapor at constant total pressure raises the melting temperature. At constant pressure, the feldspars melt completely at one temperature in the binary systems feldspar—water ($Ab_{70}Or_{30}$ is the composition of the minimum in the system albite—orthoclase), but in the ternary systems feldspar—water—carbon dioxide the feldspars pass through a melting interval at constant pressure.

Preliminary runs made with synthetic feldspars using 0.05 cc and 0.1 cc water indicate similar results. However, the PT conditions required were too high for the melting curves to be completely determined. Results obtained using 0.05 cc water are listed in table 2 and are plotted in figure 2.

DISCUSSION

The qualitative results obtained are: (1) The rates of melting and crystallization of silicate mixtures in the presence of dry carbon dioxide are very slow, (2) dry carbon dioxide under pressure apparently has little effect on the melting temperatures of granite and feldspars, and (3) the melting temperatures of granite and feldspar are raised in the presence of water and carbon dioxide at fixed total pressure when the proportion of carbon dioxide in the vapor phase is increased. The depression of melting temperatures in the presence of a volatile material depends upon the solubility of the material in the liquid—the greater the solubility, the greater the depression of the melting temperature. From the results we may conclude that the solubility of carbon dioxide in granitic and feldspathic liquids is less than that of water.

TABLE 2

Results of Melting Experiments in the Systems
Albite—Water—Carbon Dioxide and $Ab_{70}Or_{30}$—Water—Carbon Dioxide

Abbreviations: psi = pounds per square inch; xls = crystals; gls = glass

0.05 cc water plus carbon dioxide pressure			
Pressure psi	Temp. °C	Time Hrs.	Result
Starting material albite crystals			
2,000	1050	3	xls
3,000	1045	2	xls + gls
6,500	985	3	xls
14,500	930	3	xls
14,500	1000	3	gls
20,000	940	3	xls
20,000	965	3	xls + gls
Starting material $Ab_{70}Or_{30}$ crystals			
2,850	980	3	xls
3,700	990	5	xls + gls
3,000	1045	2	gls
6,000	980	5	xls + gls
15,000	890	2	xls
14,500	930	2	xls + gls

Moreover, results (1) and (2) suggest that the solubility of carbon dioxide is very low. A few experimental studies involving water and carbon dioxide at elevated pressures and temperatures are available for comparison with these results.

In a brief note England and Adams (1951) recorded some preliminary experiments on the melting behavior of silicate mixtures in the presence of carbon dioxide under pressure. They made several runs with a sample of kimberlite at temperatures up to 1290°C and pressures up to 1600 atmospheres. Carbon dioxide at various pressures had no noticeable effect on the melting behavior of the kimberlite.

Morey and Fleischer (1940) presented quantitative data on the distribution of carbon dioxide and water between liquid and vapor within the system K_2O—SiO_2—H_2O—CO_2 at a temperature of 500°C and pressures up to 412 atmospheres. The compositions of the melts were calculated in terms of molecules such as K_2SiO_3, $K_2Si_2O_5$, etc., and K_2CO_3. As carbon dioxide was added to the system K_2O—SiO_2—H_2O, most of it remained in the liquid until a definite proportion of carbonate was formed (without crystallization) in the liquid, after which the carbon dioxide remained in the vapor. Up to this limiting value, carbon dioxide was rapidly taken up by the melt, but beyond the limiting value it was less soluble in the melt than in the water vapor. With increasing SiO_2:K_2O ratio the solubilities of both carbon dioxide and water decreased, but that of carbon dioxide decreased much more rapidly. Granitic and feldspathic liquids have high SiO_2:alkali ratios and the solubility of carbon dioxide in these liquids is low.

When carbon dioxide can dissolve in a melt with the formation of carbonates, the depression of melting temperatures is considerable. For instance CaO melts at 2580°C, but in the system CaO—CO_2 at 1000 bars pressure $CaCO_3$ melts congruently at 1339°C (Smyth and Adams, 1923). Similarly, the joint effect of water vapor and carbon dioxide is greatly enhanced when they both have a tendency to form compounds with cations in the melt. In the system CaO—CO_2—H_2O at 1000 bars a liquid having the composition $CaCO_3$ = 42, $Ca(OH)_2$ = 53, H_2O = 5 in weight per cent is in stable equilibrium with a vapor, calcite, and portlandite at 675°C (Wyllie and Tuttle, 1959).

The depression of silicate melting temperatures by volatile materials such as water and fluorine can be explained structurally because hydroxyl and fluorine ions are capable of breaking oxygen bridges (Si—O—Si) in the silicate network (Buerger, 1948), but we would not expect carbon dioxide to behave in the same way. Morey and Fleischer (1940) showed that carbon dioxide is soluble in potassium silicate liquids only up to the limit of carbonate formation within the liquid. The carbon dioxide solubility increases with increasing K_2O:SiO_2 ratio, suggesting that this limit may depend upon the proportion of cations which are not structurally bound to the silicate network of the liquid. We suggest, tentatively, that the low solubility of carbon dioxide in granitic and feldspathic liquids is due to the fact that they probably contain only a small proportion of cations which are not structurally bound to the aluminosilicate networks of the liquids, i.e., there is only a small proportion of cations available for carbonate formation within the liquids.

PETROLOGIC CONSIDERATIONS

These qualitative results indicate that carbon dioxide alone is only slightly soluble in granitic liquids. The general absence of calcite or carbonates in granites is a further indication that carbon dioxide is not greatly soluble in

granite magmas. Carbonates are common in nepheline-bearing rocks and although we have not studied these alkali-rich compositions, it is to be expected from the work of Morey and Fleischer (1940) that carbonates will have a greater solubility in alkaline magmas. Alkaline igneous rocks are often accompanied by carbonatites which are believed by many petrologists to represent residual liquids formed by the crystallizing alkaline magma (Pecora, 1956). It is possible that carbon dioxide becomes more soluble in these alkaline liquids with progressive crystallization of the magma, producing a complete transition from normal alkaline magmas to carbonatite liquids.

It is also possible that the presence of water vapor in silicate melts will promote the solubility of carbon dioxide (our results using a mixture of carbon dioxide and water tell us only that carbon dioxide is less soluble than water under the conditions of the experiments), in which case, carbon dioxide will dissolve in granitic magmas during the later stages of crystallization when the water content is high. Carbon dioxide vapor brought into contact with a hydrous granitic magma which is emplaced at a temperature below its anhydrous liquidus will tend to dehydrate the liquid and induce crystallization. The dehydration may actually cause rapid crystallization, producing a quenching effect along the contacts. The hypersolvus granite dikes in limestone at Marble Delta, Port Shepston, Natal, and at Beinn an Dubhaich, Skye, Scotland and the hypersolvus border facies at many granite-limestone contacts may represent examples of carbon dioxide vapor dehydration.

In summary, although carbon dioxide is believed to be an important volatile constituent of magmas, its behavior is quite different from that of water. In the case of granitic liquids, it may be considered to act as a piston imparting pressure to the magma but not entering into it to any great extent.

ACKNOWLEDGMENT

The authors are indebted to the National Science Foundation for support of this investigation.

REFERENCES

Buerger, M. J., 1948, The structural nature of the mineralizer action of fluorine and hydroxyl: Amer. Mineralogist, v. 33, p. 744-747.

England, J. L. and Adams, L. H., 1951, Effect of carbon dioxide on melting behavior of natural rocks: Carnegie Inst. of Wash. Year Book, no. 50, p. 49.

Harker, R. I., 1958, The system MgO—CO_2—A and the effect of inert pressure on certain types of hydrothermal reaction: Am. Jour. Sci., v. 256, p. 128-138.

Harker, R. I. and Tuttle, O. F., 1955, Studies in the system CaO—MgO—CO_2, Part I. The thermal dissociation of calcite, dolomite and magnesite: Am. Jour. Sci., v. 253, p. 209-224.

Morey, G. W. and Fleischer, M., 1940, Equilibrium between vapor and liquid phases in the system CO_2—H_2O—K_2O—SiO_2: Geol. Soc. America Bull., v. 51, p. 1035-1058.

Pecora, W. T., 1956, Carbonatites: A review: Geol. Soc. America Bull., v. 67, p. 1537-1556.

Smyth, F. H. and Adams, L. H, 1923, The system calcium oxide-carbon dioxide: Am. Chem. Soc. Jour., v. 45, p. 1167-1184.

Tuttle, O. F., 1949, Two pressure vessels for silicate-water studies: Geol. Soc. America Bull., v. 60, p. 1727-1729.

Tuttle, O. F. and Bowen, N. L., 1958, Origin of granite in the light of experimental studies in the system $NaAlSi_3O_8$—$KAlSi_3O_8$—SiO_2—H_2O: Geol. Soc. America Mem. 74.

Tuttle, O. F. and Wyllie, P. J., 1957, Hydrothermal studies in the systems $NaAlSi_3O_8$ (albite)—H_2O—HF and granite—H_2O—HF (Abstract): Geol. Soc. America Bull., v. 68, p. 1807.

Wyllie, P. J. and Tuttle, O. F., 1957, The effect of volatile materials on the melting temperatures of silicates (Abstract): Am. Geophys. Union Trans., v. 38, p. 413-414.

————, 1959, Melting of calcite in the presence of water: Am. Mineralogist, v. 44, p. 453-459.

[American Journal of Science, Vol. 257, November 1959, P. 656-667]

THE SYNTHESIS AND STABILITY OF TILLEYITE, $Ca_5Si_2O_7(CO_3)_2$

R. IAN HARKER

Johns-Manville Research Center, Manville, New Jersey

ABSTRACT. At 5,000 lbs/in.^{2} of CO_2 tilleyite is stable between 930 and 970°C and at 3,000 lbs/in.^{2} of CO_2 between 870 and 930°C. The conditions of its stability are defined, on a P_{CO_2}-T diagram, by a narrow band lying between the more carbonated calcite + wollastonite assemblage and the less carbonated spurrite.

Under the conditions of the experiments it was found that traces of alumina and fluoride were necessary to effect the synthesis of tilleyite. A consideration of natural mineral assemblages currently supports the evidence that the presence of these two components is very effective in promoting the formation of tilleyite. With sufficient alumina the formation of gehlenite can be detected in apparent equilibrium with calcite + wollastonite, tilleyite or spurrite.

INTRODUCTION

Tilleyite, $Ca_5Si_2O_7(CO_3)_2$, was discovered in 1933 at Crestmore (Larsen and Dunham, 1933; Dunham, 1933) and has since been described from other contact altered limestones in four different localities. These are New Mexico (Glass, Jahns and Stevens, 1944), Carlingford (Nockolds, 1947) Camus Mor (Tilley, 1947) and Camasumary (Wyatt, 1953). It is clearly a rarer mineral than spurrite, $5CaO.2SiO_2.CO_2$, which is also characteristic of certain contact altered limestones.

Tilleyite was incorporated into Bowen's (1940) decarbonation series by Nockolds (1947) and with Tilley's (1942) discovery of rankinite the progressive contact metamorphism of a limestone, with some siliceous impurity, or into which some silica was introduced metasomatically, is now represented by the following steps:

(1) Calcite + Quartz $\rightleftarrows$ Wollastonite + CO_2
(2) Calcite + Wollastonite $\rightleftarrows$ Tilleyite + CO_2
(3) Tilleyite $\rightleftarrows$ Spurrite + CO_2
(4) Wollastonite + Spurrite $\rightleftarrows$ Rankinite + CO_2
(5) Rankinite + Spurrite $\rightleftarrows$ Larnite + CO_2 (Tilley, 1951)

EXPERIMENTATION AND RESULTS

Previous work.—Using Tuttle cold-seal pressure vessels it was found possible to investigate reaction (1) in the laboratory and to obtain equilibrium P_{CO_2}-T data for it (Harker and Tuttle, 1956). Attempts to study reactions (2) and (3) were thwarted by the failure of tilleyite to form in any of the experiments. A P_{CO_2}-T curve was obtained, however, for the reaction: Calcite + Wollastonite $\rightleftarrows$ Spurrite + CO_2 (Tuttle and Harker, 1957) and it appeared that this represented a true equilibrium because the reaction was reversible. The reason for the failure of a tilleyite + CO_2 assemblage to appear over a temperature range between that covered by the calcite + wollastonite and the spurrite + CO_2 assemblages was unknown.

The synthesis of tilleyite.—Through the kind cooperation of Professor Tilley and Dr. Nockolds, an analyzed sample of natural tilleyite from Ireland

was made available for further experiments. J. Scoon's analysis gave SiO_2 = 24.39, Al_2O_3 = 0.23, Fe_2O_3 = 0.08, MgO = 0.21, CaO = 57.01, CO_2 = 17.23, H_2O (+) = 0.62, percent. The results of some of these experiments are shown in table 1 (runs 1 to 31). After 30, 172, 242 and 329 hours at 930°C and 4,000 to 4,200 lbs/in.^{2} of CO_2 the natural material was unchanged. At somewhat higher temperatures tilleyite broke down to spurrite and at somewhat lower temperatures to calcite + wollastonite in approximately 40 hours. This suggested that tilleyite might well have a field of stability on the low temperature side of the previously determined spurrite + CO_2 stability field.

However in the region in which the natural tilleyite appeared unchanged even after long runs, calcite and silica in the ratio of 5:2 always yielded calcite + wollastonite + CO_2. Attempts to produce tilleyite by changing the $CaO:SiO_2$ ratio by up to 5 percent to values on either side of 5:2 and by adding 4 percent ferrous oxalate were of no avail and efforts to flux the reaction with a trace of water, by using a hydrated silica, were also useless. Tilleyite was finally crystallized, however, both from calcite + wollastonite and from spurrite + CO_2 when these starting materials themselves had been formed by the controlled breakdown of natural tilleyite, (runs 29, 30 and 32).

It was noted that tilleyite-bearing rocks invariably contain some alumina bearing mineral and Professor Tilley (personal communication) has observed that fluorine, in fluorite, cuspidine or idocrase, is commonly present where

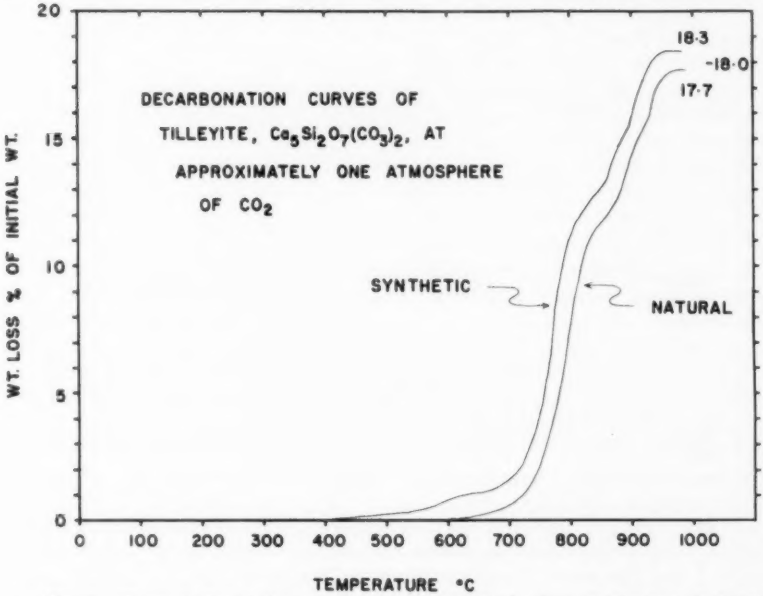

Fig. 1. Thermal dissociation curves of Natural Tilleyite from Carlingford, Ireland, (Material provided by Professor C. E. Tilley), and of Synthetic Tilleyite, (from run 65, see Table 1). The runs were carried out at one atmosphere in a continuously recording thermobalance. Tilleyite ideally contains 18.0% CO_2.

tilleyite develops (see table 2). At his suggestion runs were made with varying percentages of calcium fluoride included in aluminous starting materials. As a result tilleyite could be produced reliably from a variety of starting materials including calcite + quartz, calcite + amorphous silica and oxide mixes, within the stability range indicated by the behavior of the natural tilleyite. Experiments in this range using starting materials containing up to 8.6 percent Al_2O_3 with no CaF_2 resulted in the formation of gehlenite, with calcite + wollastonite. Starting materials with fluoride additive, but no alumina, produced no tilleyite but with sufficient fluoride an unidentified phase made its appearance.

The optical properties of a synthetic tilleyite made from a calcite + quartz mixture with 8.95 percent Al_2O_3 and 2.25 percent CaF_2 are as follows: $\alpha = 1.604 \pm .003$, $\beta = 1.630 \pm .004$ and $\gamma = 1.653 \pm .003$. Similar measurements on the material from Carlingford gave $\alpha = 1.599$, $\beta = 1.632$ and $\gamma = 1.656$. Figure 1 shows the thermal decarbonation curves of the natural and synthetic tilleyites at atmospheric pressure in a covered crucible and at a heating rate of approximately 8°C/min. The x-ray powder diffraction patterns of natural and synthetic tilleyites can be compared in figure 2.

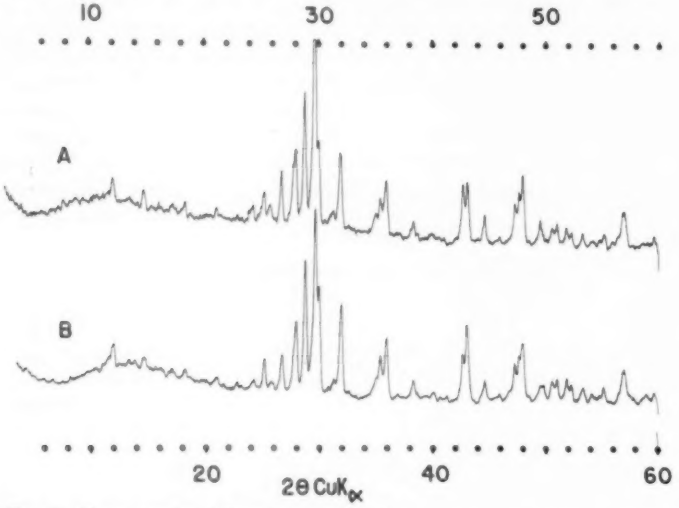

Fig. 2. X-ray powder diffraction patterns of
(A) Natural Tilleyite from Carlingford, Ireland. (Material provided by Professor C. E. Tilley).
(B) Synthetic Tilleyite, (from run 65, see Table 1).

Stability of tilleyite in the presence of excess CO_2.—The experiments from which it has been possible to outline the stability field of tilleyite are listed in table 1 and the results plotted in figure 3. The starting materials "CAS gel" indicate those made by gelling, drying and carefully igniting ethanolic mixtures of ethyl orthosilicate, calcium nitrate and aluminum nitrate solutions, (after Roy, 1956). The lime:silica ratio was always 5:2 but the alumina con-

tent was varied as indicated under "Starting Materials". The final compositions of the samples derived from these gels were spot checked analytically. Calcium fluoride was added subsequently. The products were identified by x-ray powder diffraction and/or optical examination.

In all but selected runs the pressure vessels were raised to operating conditions as quickly as possible by preheating the furnaces. In order to supress the development of calcite + wollastonite or spurrite with rising temperature the CO_2 pressure was raised with the temperature to maintain conditions about 30°C on what is believed to be the low temperature side of the spurrite stability field. By a rough extrapolation of the tilleyite $\rightleftarrows$ spurrite + CO_2 curve (assuming ideality for the CO_2 and plotting log p against 1/T) the equilibrium CO_2 pressure at about 700°C is probably only a few hundred lbs/in.^{2}. The P-T conditions of the pressure vessels even during initial heating were thus probably always in or close to the tilleyite field, at least above 700°C.

In a few selected runs, the pressure vessels were brought up to temperature and pressure purposely through stability fields other than those in which they were finally run. In runs 49 to 52 inclusive the temperature was raised before the pressure. It is felt that the trace of tilleyite found in 51 must be left over from material formed as the P-T conditions passed through the tilleyite field. In runs 53 to 56, the pressure was raised before the temperature, and the P-T conditions were held at 4,000 lbs/in.^{2} CO_2 and 907°C for 72 hours before being raised into the tilleyite field.

Altogether thirty-seven separate starting materials were made up of various kinds and with varying amounts of alumina and fluoride. Most of these were of the gelled type because in such the alumina appeared to be in a more active state than when it was mixed separately as an oxide powder. This is illustrated by some of the runs in which a *mixture* of calcite and quartz was used as the basic starting material with various amounts of alumina and calcium fluoride admixed mechanically. Runs 63 and 78 failed to produce tilleyite but *gelled* starting material with no more of the additives succeeded.

It appears that the stability of tilleyite is not appreciably changed by varying the amounts of these two additives above about 0.2 percent of each. It may be observed, however that with only these small amounts complete conversion to tilleyite was effected in only one run, (number 65) close to the center of the tilleyite field. This same starting material was only converted partially to tilleyite in runs 45 and 73 when starting materials containing a slightly higher percentage of the additives were converted largely to tilleyite under the same conditions. In runs 53, 54, and 55 some tilleyite was produced by those starting materials with the greater amounts of additives whereas 56 with only 0.2 percent of each failed to produce any detectable amounts of tilleyite. On the basis of these few runs it is very tentatively suggested that the minimum amounts of alumina and fluorine necessary for tilleyite formation, in the P-T range covered by these experiments, are 0.2 and 0.1 percent respectively.

The P_{co_2}-T curve for the reaction tilleyite $\rightleftarrows$ spurrite + CO_2 plotted in figure 3 is at somewhat lower temperatures at 5,000 lbs/in.^{2} of CO_2 than the published curve for the reaction calcite + wollastonite $\rightleftarrows$ spurrite + CO_2

(Tuttle and Harker, 1957, fig. 1). However some doubt has been cast on the exact location of the upper part of the previously published curve as runs 4 and 5 of the present work are not in agreement with it. In view of conflicting evidence it is concluded that the lower limit of stability of spurrite at 5,000 lbs/in.^{2} of CO_2 is approximately 970°C. Within the limits of error, therefore, it appears that the lower limit of stability of spurrite coincides with the upper limit of stability of tilleyite.

Role of alumina and fluoride additives.—The introduction of the two components Al_2O_3 and CaF_2 into the system $CaO—SiO_2—CO_2$ could complicate the equilibria under consideration in two ways. First, with the introduction of fluorine at such high temperatures there is the possibility of creating a heterogeneous volatile phase (Brisi, 1957). With larger amounts of fluorine this might be the case. However in the runs significant to the stability of tilleyite the amounts were very small. Considering the size of the samples and the volume of the heated pressure chamber F_2:CO_2 was approximately 1:400, by weight. At higher ratios, up to 1:20, producing appreciable amounts of the "X" phase, the results of runs of variable duration did not change the apparent stability of the carbonate phases as would be expected had this been an important factor, (see Harker, 1958).

Second, the addition of alumina and fluorine theoretically changes the variancy of the P_{co_2}-T curves of figure 3. However it appears that only very small amounts of Al_2O_3 and F_2 are necessary for the formation of tilleyite. As

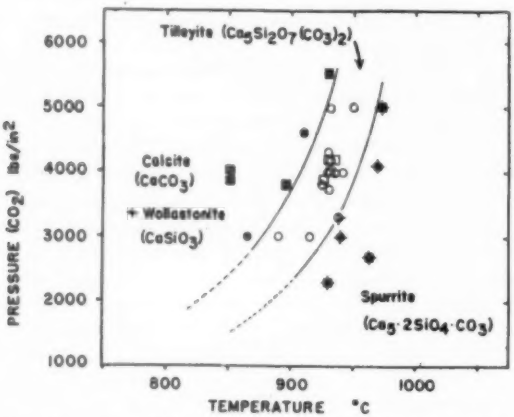

Fig. 3. P_{co_2}-T curves outlining the field in which Tilleyite + CO_2 assemblages are stable.

Square symbols indicate experiments carried out using Natural Tilleyite. Circular symbols indicate experiments carried out using Analytical Reagents.

little as 0.2 percent of Al_2O_3 and 0.1 percent F_2 suffice. Moreover under the conditions of these experiments tilleyite does not show any evidence of accepting major amounts of these components into its structure. With more than 2 percent of each, extra phases, gehlenite and "X", are evident in appreciable

amounts. Furthermore no significant difference in lattice spacings could be found between the natural specimen with 0.2 percent Al_2O_3, and a synthetic tilleyite grown from a starting material with 0.2 percent Al_2O_3 and 0.2 percent CaF_2, and a synthetic tilleyite grown from a starting material with 8.18 percent Al_2O_3 and 4.75 percent CaF_2 (see table 3). It can be assumed therefore that within the limits of experimental error the P_{co_2}-T curves are univariant.

It is of interest to note that throughout the range of these experiments alumina always appeared as gehlenite. Grossularite was not expected as the runs were all above 850°C (Roy and Roy, 1957). Compared with Yoder's (1950) decarbonation series in an argillaceous limestone it is evident that between 3,000 and 5,000 lbs/in.^{2} of CO_2, a wollastonite-calcite-gehlenite assemblage is formed before the development of tilleyite. At lower CO_2 pressures tilleyite might be expected to form at lower temperatures, over longer periods and in the presence of appreciable water, because of its occasional association with grossularite.

CONCLUSIONS AND PETROLOGIC CONSIDERATIONS

The one analysis of natural tilleyite shows 0.2 percent Al_2O_3 and no fluorine. It may be that fluorine is only acting as a mineralizer. Its mineralizing action is well illustrated by a comparison of run 34, in which 8.6 percent Al_2O_3 was present, with some of the subsequent shorter runs with less alumina but some fluoride, e.g. 36, 61, 62, 70, etc. In these later runs the gehlenite is well crystallized and easily seen under the microscope and in the x-ray patterns of the products. In 34 it is very poorly crystallized. It is thus more difficult to imagine the alumina purely as a catalyst and it is suggested that the trace that was needed for the tilleyite synthesis could hold an important place in the structure by substituting for an occasional silicon atom while a fluorine atom takes the place of an oxygen. However the amounts involved are very small and it would be difficult to prove this.

Whether or not the alumina or fluorine enter the tilleyite structure to any extent it is clearly evident that the influence of these two components in very small amounts is extremely favorable to the formation of tilleyite. Some petrographic evidence in support of this is found at Scawt Hill where spurrite occurs but where tilleyite and fluorine bearing minerals are apparently absent, (Professor Tilley, personal communication). It will be interesting to see if tilleyite and fluorine bearing minerals are present together or absent together in the spurrite bearing rocks (1) of the Tres Hermanas Mountains, New Mexico, presently being studied by Homme and Rosenzweig (1958), and (2) of the metamorphosed Onerahi limestone near Tokatoka, New Zealand (Mason, 1957).

There are at least two localities where tilleyite might be expected although its occurrence has not yet been reported. These are in the contact altered limestones some 250 km from the mouth of the Nishanaya Tunguska River in Russia, (Sobolev, 1935) and in the skarns in the central part of the Christmas Mountains, Texas (Clabaugh, 1953). In both these localities the metamorphic grade must at least have been high enough to produce tilleyite in the aureole, for spurrite occurs in the contact rocks. Furthermore both alumina and fluorine bearing minerals are present.

The position of tilleyite in the decarbonation series is where it would be expected from its CO_2 content relative to the calcite + wollastonite and spurrite assemblages. The tilleyite facies lies only one step beyond the wollastonite-calcite facies. However, this step is a large one, about 330°C at 5,000 lbs/in.^{2} of CO_2 and if the formation, or preservation, of tilleyite depends on the presence of specific foreign components, its rarity in nature is readily understood. Moreover the tilleyite stability field is narrow on a P_{co_2}-T diagram and in nature is likely to be confined to relatively narrow metamorphic zones. Unlike spurrite which may be stable with higher index minerals, such as rankinite and larnite, the stability of tilleyite (+ CO_2), per se, is limited to the field indicated in figure 3. It may well be regarded as the most sensitive of all single index minerals in the decarbonation series.

The absence of tilleyite at granite-limestone contacts is as significant as the absence of spurrite, as far as CO_2 pressures are concerned, (Tuttle and Harker, 1957, p. 232). It appears likely that even at high total pressures the *effective* partial pressure of CO_2 will be lowered in proportion to the H_2O:CO_2 ratio by weight in the fluid phase (Harker, 1958). This means that at granite-limestone contacts a relatively high CO_2 pressure is normally maintained preventing the formation of tilleyite, and higher grade minerals, which, at very low CO_2 pressures should be able to form, with sufficient time and mineralizers, at much lower temperatures.[1] There is apparently insufficient water emanating from the granites to flush out the CO_2 in the country rocks. Such evidence is difficult to reconcile with concepts involving the metasomatic enplacement of granites in which hydrous fluids (ichors) allegedly sweep through large volumes of country rock.

ACKNOWLEDGMENTS

The synthesis of tilleyite resulted from an application of the ideas and material of Professor C. E. Tilley to the equipment designed by Dr. O. F. Tuttle. The author is also indebted to the staff of the Johns-Manville Research Center for their encouragement and assistance and especially to Messrs. J. P. Pellicane, Jr. and J. P. McGourty.

REFERENCES

Bowen, N. L., 1940, Progressive metamorphism of siliceous limestone and dolomite: Jour. Geology, v. 48, p. 225-274.

Brisi, C., 1957, Role of cuspidine ($3CaO.2SiO_2.CaF_2$) in the system CaO—SiO_2—CaF_2: Am. Ceramic Soc. Am., v. 40, p. 174-178.

Clabaugh, S. E., 1953, Contact metamorphism in the Christmas Mountains, Brewster County, Texas: Geol. Soc. America Bull., v. 64, p. 1408.

Dunham, K. C., 1933, A note on the texture of the Crestmore contact rocks: Am. Mineralogist, v. 18, p. 474-477.

Glass, J. J., Jahns, R. H., and Stevens, R. E., 1944, Helvite and danalite from New Mexico and the Helvite Group: Am. Mineralogist, v. 29, p. 163-191.

Harker, R. I. and Tuttle, O. F., 1956, Experimental data on the P_{co_2}-T curve for the reaction: calcite + quartz $\rightleftarrows$ wollastonite + carbon dioxide: Am. Jour. Sci., v. 254, p. 239-256.

Harker, R. I., 1958, The system MgO—CO_2—A and the effect of inert pressure on certain types of hydrothermal reaction: Am. Jour. Sci., v. 256, p. 128-138.

[1] Since this work was completed McConnell (1958) has synthesized tilleyite from calcite + afwillite at temperatures of the order of 550°C and water pressures of 22,500 lbs/in.^{2}.

Homme, F. C. and Rosenzweig, A., 1958, Spurrite and monticellite skarns in the Tres Hermanas Mountains, Luna County, New Mexico: Geol. Soc. America, Bull., v. 69, p. 1586.

Larsen, E. S. and Dunham, K. C., 1933, Tilleyite, a new mineral from the contact zone at Crestmore, California: Am. Mineralogist, v. 18, p. 469-473.

McConnell, J. D. C., 1958, The hydrothermal synthesis of tilleyite in a CO_2-deficient Environment: paper read to Mineralogical Society of London November 6, 1958.

Mason, B., 1957, Larnite, scawtite and hydrogrossular from Tokatoka, New Zealand: Am. Mineralogist, v. 42, p. 379-392.

Nockolds, S. R., 1947, On tilleyite and its associated minerals from Carlingford, Ireland: Mineralog. Mag., v. 28, p. 151-158.

Roy, D. M. and Roy, Rustum, 1957, System $CaO—Al_2O_3—SiO_2—H_2O$, V1: The Grossularite—$3CaO.Al_2O_3.6H_2O$ join: Geol. Soc. America, Bull., v. 68, p. 1788-1789.

Roy, Rustum, 1956, Aids in Hydrothermal Experimentation: II Methods of Making Mixtures for Both "Dry" and "Wet" Phase Equilibrium Studies: Am. Ceramic Soc. Jour., v. 39, p. 145-146.

Sobolev, V., 1935, Redkii tip kontaktovogo metamorfizma izvestniakov. (Rare Type of Limestone Contact Metamorphism): Zapiski Vserossiiskogo Mineralogicheskogo Obshchéstva, v. 64, series 2, no. 1, p. 162-165. (See Chem. Abstracts, v. 32, p. 6202.)

Tilley, C. E., 1942, Tricalcium Disilicate (rankinite), A new mineral from Scawt Hill, Co. Antrim: Mineralog. Mag., v. 26, p. 190-196.

————, 1947, The gabbro-limestone contact zone of Camas Mor, Muck, Inverness-shire: Comptes Rendues Soc. Geol. Finlande, v. 20, p. 97-105.

————, 1951, A note on the progressive metamorphism of siliceous limestones and dolomites: Geological Mag., v. 88, p. 175-178.

Tuttle, O. F. and Harker, R. I., 1957, Synthesis of spurrite and the reaction: wollastonite + calcite $\rightleftarrows$ spurrite + carbon dioxide: Am. Jour. Sci., v. 255, p. 226-234.

Wyatt, M., 1953, The Camasumary (Skye) gabbro-limestone contact: Part 2 of Ph.D. Thesis, Cambridge University.

TABLE 1

Runs Made to Determine the Stability of Tilleyite

Run	Starting Materials	CO_2 Pressure lbs/in.^{2}	Temp °C	Duration Hrs	Products
1	Cc+SH	5,500	930	144	Cc+Wo
2	Ty (natural)	"	"	"	Ty (+Cc+Wo)
3	Ty (natural)	5,000	970	43	Sp
4	Cc+Wo	"	"	"	Sp
5	Sp	"	"	"	Sp
6	Ty (natural)	4,200	935	171	Ty
7	Cc+SH (10% extra Cc)	"	"	"	Cc+Wo
8	Cc+SH {10% extra Cc +4% $Fe(COO)_2.2H_2O$}	"	"	"	Cc+Wo
9	Ty (natural)	4,000	930	30	Ty
10	Cc+Wo	"	"	"	Cc+Wo(+Sp)
11	Sp	"	"	"	Cc+Wo
12	Ty (natural)	4,000	880	39	Ty(+Cc+Wo)
13	Cc+Wo	"	"	"	Cc+Wo
14	Sp	"	"	"	Cc+Wo
15	Ty (natural)	4,000	850	33	Cc+Wo
16	Ty (natural)	3,900	927	312	Ty
17	Cc+Wo	"	"	"	Cc+Wo
18	Sp	"	"	"	Cc+Wo
19	Ty (natural)	3,900	850	312	Cc+Wo
20	Cc+Wo	"	"	"	Cc+Wo

TABLE 1 (Continued)

Run	Starting Materials	CO_2 Pressure lbs/in.^{2}	Temp °C	Duration Hrs	Products
21	Sp	"	"	"	Cc+Wo
22	Ty (natural)	3,800	895	285	Ty+Cc+Wo
23	Cc+SH (10% extra Cc)	"	"	"	Cc+Wo
24	Cc+SH {10% extra Cc+ 4% $Fe(COO)_2.2H_2O$}	"	"	"	Cc+Wo
25	Ty (natural)	2,700	963	152	Sp
26	Ty (natural)	2,300	930	146	Ty+Sp
27	Cc+SH	"	"	"	Sp
28	Tv (natural)	4,200	932	329	Ty
29	Ty+Sp (from run 26)	"	"	"	Ty alone
30	Ty+Cc+Wo (from run 22)	4,150	937	172	Ty alone
31	Ty (natural)	4,000	930	242	Ty
32	Ty+Cc+Wo (from run 22)	"	"	"	Ty alone
33	Cc+SH+16.3% CaF_2	4,150	937	172	Cc+X
34	CAS gel (8.6% Al_2O_3)	4,200	932	329	Cc+Wo (+Ge)
35	CAS gel {(8.18% Al_2O_3)+Ty (4.75% CaF_2) seed}	4,150	937	172	Ty+X+Ge+Cc
36	As above but no seed	4,000	930	242	Ty+X+Ge+Cc
37	Ty (from run 74)	7,700	915	64½	Cc+Wo
38	CAS gel {0.2% Al_2O_3 0.2% CaF_2}	"	"	"	Cc+Wo
39	CAS gel {8.5% Al_2O_3 1.77% CaF_2}	"	"	"	Cc+Wo+Ge
40	CAS gel (1.96% Al_2O_3)	"	"	"	Cc+Wo
41	CAS gel (1.96% Al_2O_3)	5,000	930	185	Cc+Wo
42	CAS gel {0.2% Al_2O_3 0.2% CaF_2}	"	"	"	Cc+Wo(+Ty)
43	CAS gel {1.96% Al_2O_3 0.27% CaF_2}	"	"	"	Cc+Wo+Ty
44	Ty(+Cc) (from run 68)	"	"	"	Ty
45	CAS gel {0.2% Al_2O_3 0.2% CaF_2}	5,000	950	144	Ty+Cc+Wo
46	CAS gel {1.96% Al_2O_3 0.27% CaF_2}	"	"	"	Ty(+Cc+Ge)
47	CAS gel {1.93% Al_2O_3 1.83% CaF_2}	"	"	"	Ty (+Ge)
48	Ty (from run 75)	"	"	"	Ty
49	CAS gel {0.2% Al_2O_3 0.2% CaF_2}	4,600	910	240	Cc+Wo
50	CAS gel {8.18% Al_2O_3 4.75% CaF_2}	"	"	"	Cc+Ge+Wo+X
51	CAS gel {1.93% Al_2O_3 1.83% CaF_2}	"	"	"	Cc+Wo(+Ge+Ty)
52	Ty (+Ge) (from run 47)	"	"	"	Cc+Wo(+Ge)
53	CAS gel {3.7% Al_2O_3 1.4% CaF_2}	4,300	930	216	Ty+Cc+Wo+Ge(+X)

TABLE 1 (Continued)

Run	Starting Materials	CO_2 Pressure lbs/in.^{2}	Temp °C	Duration Hrs	Products
54	CAS gel {0.79% Al_2O_3, 0.75% CaF_2}	"	"	"	Cc+Wo+Ty(+Ge)
55	CAS gel {5.3% Al_2O_3, 0.9% CaF_2}	"	"	"	Cc+Wo+Ty+Ge
56	CAS gel {0.2% Al_2O_3, 0.2% CaF_2}	"	"	"	Cc+Wo
57	CAS gel {1.93% Al_2O_3, 1.83% CaF_2}	4,100	970	167	Sp(+Ge+X)
58	CAS gel {1.96% Al_2O_3, 0.27% CaF_2}	"	"	"	Sp(+Ge)
59	CAS gel {0.2% Al_2O_3, 0.2% CaF_2}	"	"	"	Sp
60	Ty (from run 75)	"	"	"	Sp
61	CAS gel {8.5% Al_2O_3, 1.77% CaF_2}	4,000	930	141	Ty+Cc+Ge(?+X)
62	CAS gel {8.18% Al_2O_3, 4.75% CaF_2}	"	"	"	Ty+X+Ge+Cc
63	Cc+Qz {0.84% Al_2O_3, 0.21% CaF_2}	4,000	930	172	Cc+Wo
64	CAS gel {0.2% Al_2O_3, 2.0% CaF_2}	"	935	"	Ty
65	CAS gel {0.2% Al_2O_3, 0.2% CaF_2}	"	940	"	Ty
66	CAS gel {1.96% Al_2O_3, 0.27% CaF_2}	3,800	925	164	Ty(+Cc+Ge,?+Wo)
67	Cc+Qz {1.85% Al_2O_3, 1.91% CaF_2}	"	"	"	Ty(+Cc+Ge,?+Wo)
68	CAS gel {0.98% Al_2O_3, 1.94% CaF_2}	"	"	"	Ty(+Cc)
69	CAS gel {1.93% Al_2O_3, 1.83% CaF_2}	"	"	"	Ty(+Cc+Ge)
70	Cc+Qz {8.95% Al_2O_3, 2.25% CaF_2}	3,750	930	240	Ty+Cc+Ge+X
71	CAS gel {1.93% Al_2O_3, 1.83% CaF_2}	"	"	"	Ty+Cc(+Ge,?+X)
72	CAS gel {8.5% Al_2O_3, 1.77% CaF_2}	"	"	"	Ty+Cc+Ge(?+X)
73	CAS gel {0.2% Al_2O_3, 0.2% CaF_2}	3,300	937	280	Ty+Sp
74	CAS gel {0.2% Al_2O_3, 2.0% CaF_2}	"	"	"	Ty
75	CAS gel {0.98% Al_2O_3, 1.94% CaF_2}	"	"	"	Ty
76	CAS gel {1.93% Al_2O_3, 1.83% CaF_2}	3,000	887	191	Ty+Cc+Wo(?+Ge)

TABLE 1 (Continued)

Run	Starting Materials	CO_2 Pressure lbs/in.^{2}	Temp °C	Duration Hrs	Products
77	CAS gel {3.7% Al_2O_3 1.4% CaF_2}	"	"	"	Cc+Wo+Ty(?+Ge)
78	Cc+Qz {8.95% Al_2O_3 2.25% CaF_2}	"	"	"	Cc+Wo+Ge+X
79	Ty (from run 64)	"	"	"	Ty
80	CAS gel {1.93% Al_2O_3 1.83% CaF_2}	3,000	915	191	Ty+Cc+Ge(+X, ?+Wo)
81	CAS gel {3.7% Al_2O_3 1.4% CaF_2}	"	"	"	Ty+Ge(?+X)
82	CAS gel {8.95% Al_2O_3 2.25% CaF_2}	"	"	"	Ty+Cc+Ge
83	Ty (from run 64)	"	"	"	Ty(+X)
84	CAS gel {0.2% Al_2O_3 0.2% CaF_2}	3,000	940	459	Sp
85	CAS gel {8.98% Al_2O_3 4.75% CaF_2}	"	"	"	Sp+Ge+X
86	CAS gel {1.93% Al_2O_3 1.83% CaF_2}	"	"	"	Sp(+Ge+X)
87	Ty(+Ge) (from run 47)	"	"	"	Ty+Sp
88	Ty(+Ge) (from run 47)	3,000	865	650	Cc+Wo(+X+Ge)
89	CAS gel {1.93% Al_2O_3 1.83% CaF_2}	"	"	"	Cc+Wo(+X+Ge)
90	CAS gel {8.98% Al_2O_3 4.75% CaF_2}	"	"	"	Cc+Wo+Ge+X
91	CAS gel {3.7% Al_2O_3 1.4% CaF_2}	"	"	"	Cc+Wo(+Ge, ?+X)

Table 1—Runs made with C:S ratios on or close to tilleyite ($5CaO:2SiO_2$).

CAS gel = Anhydrous oxide mixture prepared from gel (see text).

Cc = Calcite

Ty = Tilleyite

Wo = Wollastonite

Ge = Gehlenite

Sp = Spurrite

X = Unidentified phase

Qz = Quartz

SH = SiO_2nH_2O (87.64% SiO_2).

( ) = Trace of material indicated.

TABLE 2

Natural Occurrences of Tilleyite and the Minerals Associated with it

Crestmore (Larsen and Dunham, 1933)	Tilleyite, Merwinite, Vesuvianite, Grossularite, Wollastonite, Spurrite, Gehlenite
New Mexico (Glass, Jahns and Stevens, 1944)	Tilleyite, Vesuvianite, Andradite, Magnetite, Fluorite
Carlingford (Nockolds, 1947)	Tilleyite, Melilite, Calcite Vesuvianite, Spurrite, Melilite, Tilleyite
Camus Mor (Tilley, 1947)	Spurrite, Tilleyite, Calcite, Grossularite Gehlenite, Tilleyite, Calcite, Spurrite (Cuspidine)
Camasumary (Wyatt, 1953)	Tilleyite, Spurrite, Wollastonite, Melilite (Cuspidine)

TABLE 3

Observed (CuKα) Spacings and Intensities for

1) Natural Tilleyite, 2) Synthetic Tilleyite (run 65, with 0.2% Al_2O_3 and 0.2% CaF_2) and 3) Synthetic Tilleyite (run 62, with 8.18% Al_2O_3 and 4.75% CaF_2; *peaks much weakened or suffering interference from the excess of gehlenite and the "X" phase have been omitted).

1) Natural Tilleyite		2) Synthetic Tilleyite		3) Synthetic Tilleyite		
d spacings Å	Relative Intensity	d spacings Å	Relative Intensity	d spacings Å	Relative Intensity	Estimated Accuracy of d
7.33	10	7.34	13	7.35	20	± 0.01
5.99	7	5.99	9	*		± 0.01
4.21	3	4.22	7	*		± 0.01
3.674	3	3.673	4	*		± 0.01
3.534	13	3.534	23	3.532	20	± 0.004
3.453	5	3.452	7	3.450	8	± 0.004
3.335	22	3.333	29	3.331	24	± 0.003
3.214	20	3.210	19	3.214	14	± 0.003
3.190	32	3.191	47	3.192	40	± 0.003
3.099	61	3.101	91	*		± 0.003
3.011	100	3.011	100	3.011	100	± 0.003
2.982	39	2.980	75	2.982	66	± 0.002
2.896	3					± 0.002
2.860	4	2.859	7	*		± 0.003
2.803	39	2.803	56	2.803	46	± 0.002
2.566	8	2.566	7	*		± 0.003
2.535	16	2.536	18	2.537	26	± 0.003
2.501	22	2.501	31	*		± 0.002
2.350	8	2.351	10	2.354	14	± 0.002
2.248	3					± 0.004
2.119	19	2.119	22	2.119	20	± 0.002
2.100	38	2.100	43	*		± 0.002
2.032	13	2.031	13	*		± 0.002
1.942	3	1.942	4	*		± 0.002
1.926	21	1.925	26	*		± 0.002
1.910	22	1.910	22	1.911	30	± 0.002
1.896	44	1.897	39	1.895	40	± 0.002
1.840	8	1.841	10	1.840	12	± 0.001
1.831	5	1.831	9	1.831	20	± 0.003
1.804	12	1.805	16	*		± 0.001

[American Journal of Science, Vol. 257, November 1959, P. 668-672]

CARBONATE MINERALOGY OF THE LOWER ORDOVICIAN BURCHARDS LIMESTONE IN WEST-CENTRAL VERMONT

E-AN ZEN

U. S. Geological Survey, Washington 25, D. C.

ABSTRACT. The mineralogy of mottled limestones and associated dolostones of the Lower Ordovician Burchards limestone in west-central Vermont was quantitatively studied by x-ray diffraction. The dolomitic mottled patches consist of dolomite and calcite, and the bulk chemical composition calculates out consistently to about 30 percent of $MgCO_3$ by weight, which is verified by wet chemical analysis. Among the mottled patches, outlines of mollusks can be discerned locally. This fact, together with the constant chemical composition of the patches, in contrast with the nearly dolomite-free limestone matrix, suggests that the patches may be recrystallized organic debris with the magnesium derived locally from original high-magnesium calcite. The bedded nature of the Burchards further suggests a fore reef detrital origin, which agrees with present knowledge of the paleogeography of the area during Early Ordovician time.

The Burchards limestone of west-central Vermont, whose stratigraphic relations are discussed in another contribution (Cady and Zen, in preparation), has been studied mineralogically in an effort to understand its origin. The dolomite-mottled limestone, the associated massive dolostone, and also limestone and dolostone from the adjacent Weybridge member, have been collected from the Seager Hill-Willow Brook area in the vicinity of Brandon.

On a fresh surface, the dolomitic patches of the Burchards limestone can be distinguished, by their olive-gray color and coarser grain size, from the aphanitic, dark grey "matrix". The weathered surfaces of the dolomitic patches are smooth and yellow-gray in color, and of the "matrix", light bluish gray. Rarely, gastropod and brachiopod forms can be identified and associated with the dolomitic patches on weathered surfaces. The two rock types can also be distinguished in thin sections, as the "matrix" is much darker and finer grained; the dolomitic patches, in rare instances, show curved outlines of fossil remains, some of which are brachiopods, but which generally cannot be recognized.

Samples of the two lithologies were obtained by careful drilling of the specimens. The x-ray data on these, and on the other rock types, are given in table 1. The (10.4) spacings of calcite and dolomite were measured on the Norelco diffractometer at a goniometer speed of ¼° per minute and chart speed of ½″ per minute; quartz was used as internal standard, $2\Theta_{CuK\alpha}$ (10.1) quartz = 26.664. For estimating the relative amounts of the two carbonates in a given sample, the method and calibration curves of Schmalz (1958) were used. Schmalz's method may be applied in two ways: either (1) by direct fixed-time counting of the reflected intensities at peak positions, with standardized corrections for the background, or (2) by measuring the peak height above background on the x-ray charts. Results using the latter method are given in tables 1 and 3 in parentheses.

Within limits of experimental error, estimated at ± 0.002Å, there is no difference between spacings of dolomite from the "matrix" and from the dolomitic patches, nor among different specimens. The same is true of calcite. This

is understandable, since all but one sample contain both carbonates, and during regional metamorphism (Zen, in press) these carbonates, collected from a limited area, presumably have attained mutual chemical equilibrium and ought to show the same lattice spacings. X-ray fluorescence analyses on specimens 1162-1 and 1955-2 show their iron content to be negligible and manganese to be absent, both in the "matrix" and in the dolomitic patches. The lattice spacings also suggest that both calcite and dolomite are nearly pure $CaCO_3$ and $CaMg(CO_3)_2$, respectively.

Assuming that iron is absent and the phases are stoichiometric, the relative weight percents of $MgCO_3$ and $CaCO_3$ in the samples can be calculated. These are given in the last two columns of table 1. It is seen that errors of a few percent in the relative amounts of the two carbonates will not lead to large errors in the bulk chemical composition.

The dolomitic patches of the Burchards limestone are quite constant in composition, having about 70 percent of $CaCO_3$ by weight. The "matrix" is uniformly low in $MgCO_3$, although a dolomite phase is generally present. The other rock types show no consistent trend, although the massive dolostones show the highest $MgCO_3$ content. A partial chemical analysis of the dolomitic patches of specimen 1162-1 is given in table 2, with the calculated weight percents of $CaCO_3$ and $MgCO_3$. The agreement with x-ray data is remarkable.

In table 3 are listed for comparison the x-ray chemical data on a number of Lower- to Middle-Ordovician carbonate rocks from adjacent areas. Among the specimens, numbers 1, 2, and 7 require comment. Specimen no. 1 is lithologically identical with the Burchards type of the Willow Brook area and shows an internal cast of a gastropod on the weathered surface. The two lithologies are hard to distinguish in the fresh sample, however, and mutual contamination during drilling was possible. The dolomite content of the dolomitic patch and the "matrix", therefore, must be taken as minimal and maximal values, respectively. Specimen no. 2, from Fort Cassin, is correlative of the Burchards limestone (W. M. Cady, letter, May, 1958). Where broadly similar in lithology, however, the dolomitic patches are olive-brown on fresh surfaces and weather into light gray, slightly sandy areas, quite distinct from the typical Burchards of the Willow Brook area. They may not represent the same kind of material. It is thus interesting to note that data from specimen no. 1 agree with those from the Willow Brook area, whereas data from specimen no. 2 do not.

Specimen no. 7 is included because it contains the fossil *Girvanella* (?) which is supposed to be a calcareous alga. X-ray data show however that the fossil form contains no detectable dolomite and therefore it is presumably low in the $MgCO_3$ content as well.

Cady and Zen (in preparation) suggest a reef-origin for the Burchards limestone. The high magnesium content of the dolomitic patches might correspond to high-magnesium calcite which is present in the hard parts of many reef-forming organisms (Chave, 1954a, b; Goldsmith, Graf, and Joensuu, 1955; Schmalz, 1955). High-magnesium calcite is metastable (Graf and Goldsmith, 1955; Harker and Tuttle, 1955), and during diagenesis or regional metamorphism would break up into two phases, a calcite of lower magnesium content and a dolomite. This might be the mechanism for the formation of the

TABLE 1

X-ray Data on the Burchards Limestone and Related Rocks, Seager Hill-Willow Brook Area

Sample number	Locality	*d* (10.4), ±0.002Å		Weight %		Weight % $MgCO_3$	Weight % $CaCO_3$
		Dol.	Calc.	Dol.	Calc.		
1158-1 (massive dol.)	600′ el., ¼ mi. E. of Willow Br. School	2.886	3.032	81 (83)	19 (17)	36 (38)	64 (62)
1158-2 (ls.)	Same	2.886	3.030	10 (18)	90 (82)	5 (8)	95 (92)
1162-1	550′ el., ⅛ mi. NW of 523′ road corner near Seager Hill	2.886	3.030	63 (70)	37 (30)	29 (32)	71 (68)
Dol. patch		2.887	3.032	(6)	(94)	(3)	(97)
Matrix							
1162-2	Same						
Dol. patch		2.887	3.030	(66)	(34)	(30)	(70)
Matrix		2.888	3.032	(9)	(91)	(4)	(96)
1953-1 (massive dol.)	630′ knob, 7/16 mi. SW of same road corner	2.887	3.030	(70)	(30)	(32)	(68)
1955-2	690′ knob, 3/16 mi. S of the same road corner						
Dol. patch		2.888	3.032	65 (69)	35 (31)	30 (31)	70 (69)
Matrix		—	3.032	0	100	0	100
1955-3 (massive dol.)	Same	2.887	3.032	(0) (84)	(100) (16)	(0) (38)	(100) (62)
1955-4	Along road ⅛ mi. SE of the same road corner						
Dol. patch		2.887	3.030	(64)		(36) (29)	(71)
Matrix		?	3.030	(7)		(93) (3)	(97)

TABLE 2

Partial Chemical Analysis of the Dolomitic Patches from Specimen 1162-1 (Burchards limestone from near Seager Hill near Brandon, Vermont)

J. Ito, analyst

CaO*	37.5
MgO	13.0
Fe, total, as Fe_2O_3	0.5
SiO_2	4.5
R_2O_3**	1.3

TABLE 2 (Continued)

* Spectrographic analysis shows only trace amounts of SrO and BaO in the CaO precipitate.

** Exclusive of Fe_2O_3. Spectrographic analysis shows this to be dominantly Al, Mn, Ni, Zn, and Cu but contains trace amounts of Mo, Cd, and Sn.

Spectrographic analysis of the "matrix" material from the same sample shows it contains order of 0.001% SrO.

Relative weight percents of the carbonates in the dolomitic patches:

	By chemical analysis	By x-ray
$CaCO_3$	71.1	71
$MgCO_3$	28.9	29

dolomitic patches, at least for the typical Burchards limestone of the Willow Brook area. The proposed mechanism is also suggested by Chave (1954b, p. 598) to account for some two-carbonate crinoid skeletons of Silurian and Triassic ages.

Calcareous algae were likely major reef-forming organisms during Lower Ordovician time. A modern form, *Goniolithon*, is reported by Chave (1954a, p. 273) to take up as much as 29 percent of $MgCO_3$ in solution in the calcite phase. This value is close to the 30 percent found in the dolomitic patches. Mollusk and possibly brachiopod remains in these patches, however, cannot be reconciled with Chave's data on their modern equivalents, and at least locally chemical readjustments must have occurred. The source of magnesium however may not have been outside of the rock; the sequence of phenomena here envisioned is similar to Schlanger's description (1957) of the dolomite growth of Eocene coralline algae from the Eniwetok drill core.

The presence of dolomite in the "matrix" suggests that fine particles of high-magnesium calcite may have been mixed in with the calcite at the time of deposition, thus they might correspond to a fore-reef detrital deposit, in agreement with the bedded nature of the Burchards limestone in the Willow Brook area. The dolomite may, however, be due merely to contamination by tiny dolomitic patches during the separation.

To see if one or the other of these two portions of the Burchards limestone could originally have been aragonitic, the "matrix" and the dolomitic patches were examined both by spectrographic and x-ray fluorescence methods, since any strong discrepancy in their strontium and barium contents might be correlated with the original mineralogy. X-ray fluorescence studies of specimen 1162-1 and 1955-2 show that these elements are virtually absent, both in the "matrix" and the dolomitic patches, to the limit of detection by the instrument on the untreated samples. Spectrographic results on specimen 1162-1 are given in table 2 and confirm the conclusions. The data are thus inconclusive for genetic interperetations.

I am indebted to Wallace M. Cady and Alfred H. Chidester for collecting the specimens described in table 3, and for reading the manuscript. The manuscript was also reviewed by Raymond Siever and McLain J. Forman. The material was presented at the Carbonate Symposium held under the auspices of the Geochemical Society in September, 1959; the comments from its participants are appreciated.

TABLE 3

X-ray Data on Lower and Middle Ordovician Carbonate Rocks from Cornwall, Waltham, and Ferrisburg Townships

Sample number	Locality	Description	Weight % Dol.	Weight % Calc.	Weight % $MgCO_3$	Weight % $CaCO_3$
1	1.0 mi. S of Cornwall village	Burchards ls.				
		Dol. patch, fresh	(65)	(35)	(30)	(70)
		Same, weathered	(91)	(9)	(42)	(58)
		Matrix	(4)	(96)	(2)	(98)
2	E shore of peninsula, Fort Cassin, Ferrisburg	"Reefy" ls, correlative of Burchards				
		Dol. patch	(85)	(15)	(39)	(61)
		Matrix	(3)	(97)	(1)	(99)
3	N end of peninsula, same	Gyracone from loose block near exposure of Bascom ls.				
		Shell	(84)	(16)	(38)	(62)
		Filling, black ls.	(0)	(100)	(0)	(100)
4	SW end of peninsula, same	Massive dol. between Bascom and Burchards types	(97)	(3)	(44)	(56)
5	1.0 mi. S of Cornwall village, E of road	Bridport dolomite	(86)	(14)	(39)	(61)
6	0.3 mi. S of road intersection 1.3 mi. SE of Fort Cassin	Chazyan limestone				
		Dol. patch	(68)	(32)	(31)	(69)
		Matrix	(12)	(88)	(6)	(94)
7	1.0 mi. NW of Buck Mtn., Waltham	Chazyan limestone				
		Girvanella (?)	(0)	(100)	(0)	(100)
		Matrix	(0)	(100)	(0)	(100)
8	Same as above, loose fragment	Black ls, filling of *Maclurites magnus*, Crown Point ls.	(17)	(83)	(8)	(92)

REFERENCES

Cady, W. M., and Zen, E., in preparation, Stratigraphic relationships of the Lower Ordovician Chipman formation in west-central Vermont.

Chave, K. E., 1954a, Aspects of the biogeochemistry of magnesium. 1. Calcareous marine organisms: Jour. Geology, v. 62, p. 266-283.

———, 1954b, Aspects of the biogeochemistry of magnesium. 2. Calcareous sediments and rocks: Jour. Geology, v. 62, p. 587-599.

Goldsmith, J. R., Graf, D. L., and Joensuu, O. I., 1955, The occurrence of magnesian calcites in nature: Geochim. et Cosmochim. Acta, v. 7, p. 212-230.

Graf, D. L., and Goldsmith, J. R., 1955, Dolomite-magnesian calcite relations at elevated temperatures and CO_2 pressures: Geochim et Cosmochim Acta, v. 7, p. 109-128.

Harker, R. I., and Tuttle, O. F., 1955, Studies in the system $CaO-MgO-CO_2$ part 2, limits of solid solution along the binary join $CaCO_3-MgCO_3$: AM. JOUR. SCI., v. 253, p. 274-282.

Schlanger, S. O., 1957, Dolomite growth in coralline algae: Jour. Sed. Petrology, v. 27, p. 181-186.

Schmalz, R. F., 1956, Mineralogy of the Funafuti cores and its bearing upon the physico-chemistry of dolomite (abstract): Jour. Paleontology, v. 30, p. 1004-1005.

———, 1958, A technique for quantitative modal analysis by x-ray diffraction and its application to modern sediments of the Peru-Chile Trench: Harvard University thesis, 150 p.

Zen, E., in press, Metamorphism of Lower Paleozoic rocks in west-central Vermont: Am. Mineralogist.

WILEY BOOKS

Two new Wiley books in geology . . .

PETROLEUM GEOLOGY

Second Edition

By KENNETH K. LANDES, University of Michigan. Since the publication of the first edition of *Petroleum Geology*, geology and other facets of oil finding have evolved and developed to a tremendous extent. These rapid changes in the field have caused Professor Landes to rewrite three-fourths of his material.

A major innovation in the second edition is the incorporation of a new chapter on "Reservoir Seals". Discussion on the origin and evolution of oil and gas is the most complete to be found anywhere. The role played by fractures, both in the migration and storage of oil is given considerable discussion, and the habitat of oil is covered in detail.

The greater part of the book deals with modern theories of the origin and evolution of oil and gas, rocks which contain oil and gas, associated fluids in the reservoirs, the migration of hydrocarbons through the rocks, and the various types of traps in which commercial deposits occur. 1959. 444 pages $9.50

THE SEA OFF SOUTHERN CALIFORNIA

By K. O. EMERY, University of Southern California. This book is the first and only *full-scale* treatment of the Southern California underwater area. All aspects of geology are treated and synthesized in this discussion. The author describes the tie between physiography, structure, water, life, and sediments in the ocean. He also discusses the influence of the above on the origin, migration, and accumulation of petroleum. Featuring a close tie between text and illustrations, the book contains answers to questions of interest to oil geologists and oil companies, such as the distribution of rocks of various ages off shore, the locations of oil seeps, and the heights of waves. Of more fundamental interest is the inclusion of new data on the origin of oil; the dependence of hydrocarbons on environmental factors such as production of phytoplankton, oxidation, and dilution by detrital sediment.

1959. Approx. 384 pages. Prob. $12.50

Send for examination copies today.

JOHN WILEY & SONS, Inc. 440-4th Ave., New York 16, N.Y.

VOL. 257 No. 9, 1959

American Journal of Science

NOVEMBER 1959

CONTENTS

Role of Oxygen Pressure in the Crystallization and Differentiation of Basaltic Magma ..... *E. F. Osborn* 609

Effect of Carbon Dioxide on the Melting of Granite and Feldspars *P. J. Wyllie and O. F. Tuttle* 648

The Synthesis and Stability of Tilleyite, $Ca_5Si_2O_7(CO_3)_2$ ..*R. Ian Harker* 656

Carbonate Mineralogy of the Lower Ordovician Burchards Limestone in West-Central Vermont ..... *E-an Zen* 668